MASTER THESIS

Biosensing based on magnetically induced motion of magnetic microparticles

Submitted at the Faculty of Electrical Engineering, Vienna University of Technology
in partial fulfillment of the requirements for the degree of
Master of Sciences (Diplomingenieur)

under supervision of

Ao.Univ.Prof. Dr. Franz Keplinger
Dr. Ioanna Giouroudi
Dipl.-Ing. Georgios Kokkinis

by

Alexander Dangl, BSc.
Matr.Nr. 9925845
Adolf Schmidlgasse 6/15, 1200 Wien

November, 2013

_____

Abstract

In this thesis a microfluidic biosensing device for detecting a bioanalyte (biomolecules, cells or viruses) utilizing the motion of magnetic particles (MPs) suspended in a microfluidic channel is presented. Current carrying conductors are used to move the MPs.

MPs can be functionalized by modifying their surface, thus enabling them to chemically bind to a specific (non-magnetic) analyte. These newly formed compounds are then called loaded MPs or LMPs and have a bigger overall volume than the MPs but still the same magnetic volume. MPs can be manipulated inside a microfluidic channel by exposing them to a magnetic field. Therefore it is also possible to indirectly manipulate a specific non-magnetic analyte if it is part of an LMP. If both, MPs and LMPs, are moved by the same magnetic field, the bigger LMPs are going to be slower than the MPs. This difference in velocity is used to discriminate between MPs and LMPs as LMPs will need more time to travel the same distance in comparison to MPs. Thus, when a sample liquid is analyzed and the MPs need longer to travel a distinct distance than MPs in a reference sample, the MPs in the sample under investigation must be in fact LMPs. Hence the presence of bioanalyte is proven.

Calculations concerning the velocity change of MPs, and concerning the magnetic field generated by the current carrying conductors were carried out. Simulations of various geometries for the conductors and various MPs were performed using a finite element analysis software. Several chips were fabricated and experiments with different MPs and LMPs were conducted as a proof of concept.

Kurzfassung

In dieser Diplomarbeit wird ein mikrofluidischer Biosensor-Chip zur Detektierung von Bioanalyten (Biomoleküle, Zellen oder Viren) vorgestellt der sich die Bewegung von magnetischen Partikeln (MPs) innerhalb eines mikrofluidschen Kanals zu Nutze macht. Die MPs werden dabei durch stromführende Leiter bewegt.

MPs können funktionalisiert werden indem man deren Oberfläche so verändert, dass sie chemisch einen bestimmten (nicht-magnetischen) Analyten binden. Dabei entstehen neue Körper, sogenannte loaded MPs oder LMPs, die zwar dasselbe magnetische Volumen aber ein größeres Gesamtvolumen haben. Es ist möglich MPs innerhalb eines mikrofluidischen Kanals mittels Magnetfelder zu manipulieren. Dadurch ist es auch möglich einen nicht-magnetischen Analyten indirekt zu manipulieren sofern er Teil eines LMPs ist. Wenn MPs und LMPs vom selben magnetischen Feld beschleunigt werden, erreichen die größeren LMPs nicht die Geschwindigkeit der MPs sondern bleiben langsamer. Dieser Geschwindigkeitsunterschied kann dazu benutzt werden um zwischen MPs und LMPs zu unterscheiden; LMPs brauchen länger um dieselbe Distanz zurückzulegen als MPs. Wenn also die MPs in einer zu untersuchenden Probe für eine bestimmte Distanz länger brauchen als MPs in einer Referenzprobe, dann handelt es sich bei den MPs in der zu untersuchenden Probe in Wahrheit um LMPs. Womit die Anwesenheit von Analyt in der Probe bewiesen ist.

Es wurden Berechnungen betreffend der Geschwindigkeitsänderungen der MPs und des von den stromführenden Leitern erzeugten Magnetfeldes ausgeführt. Für verschiedene Leitergeometrien und verschiedene MPs wurden Simulationen mit einer Finite Elemente Analyse Software durchgeführt. Mehrere Chips wurden produziert und Experimente mit unterschiedlichen MPs und LMPs durchgeführt.

Acknowledgments

This thesis is part of the project “On-Chip Biosensing utilizing the Motion of Magnetic Particles” sponsored by the FWF - Fonds zur Förderung der wissenschaftlichen Forschung, project number P24372-N19.

First and foremost, I would like to express my deep gratitude to my parents, Elisabeth and Stefan Dangl, for their support and love throughout my life.

I would like to express my appreciation to Ao.Univ.Prof. Dr. Franz Keplinger for the opportunity to work in such an interesting field of research. I am especially grateful to Dr. Ioanna Giouroudi and Dipl.-Ing. Georgios Kokkinis for all their support, encouragement and guidance throughout my work.

Also, I would like to thank Ing. Edeltraud Svasek and Ing. Peter Svasek for their help in device fabrication as well as all the other colleagues at the Institute of Sensors and Actuator Systems for creating such a pleasant working atmosphere.

Finally I want to thank everybody who contributed to the success of this master thesis with their technical or personal support.

Table of Contents

Nomenclature

AC	Alternating current
AZ5214	Image reversal photoresist
CCD	Charge-coupled device
CFD	Computational fluid dynamics
COOH	Carboxylic acid group
cTnI	cardiac troponin I
DC	Direct current
DI-water	Deionized water
DLVO	Derjaguin, Landav, Verwey, Overbeek
D-sub	Common type of electrical connector
Fe_3O_4	Magnetite
FEM	Finite element method
FITC	Fluorescein isothiocyanate
GUI	Graphical user interface
IDC	Insulation displacement contacts
LED	Light emitting diode
LMP	Loaded magnetic particle
MES	2-(4-morpholino)ethanesulphonic acid
MOSFET	Metal–oxide–semiconductor field-effect transistor
MP	Magnetic particle
Na_2CO_3	Sodium carbonite
NH_2	Amino group
NHS	N-hydroxysuccinimide
Ordyl SY355	Negative-type dry-film photoresist
PBS	Phosphate buffered saline
PCB	Printed circuit board
PDMS	Polydimethylsiloxane
PEB	Post-exposure bake
PET	Polyester
PT	Polyethylene
Re	Reynolds number
Si	Silicon
SiO_2	Silicon dioxide
SU-8	Epoxy-based negative photoresist
USB	Universal serial bus
UV	Ultraviolet
γ-Fe_2O_3	Maghemite

1 Introduction

In the last decades microfluidic lab-on-a-chip systems have been a fast growing field of research and they provided solutions for many problems in chemical and biological analysis. In many cases the goal is to design a portable point-of-care device operated by non-scientific personnel in order to run tests outside a laboratory environment [1]. Key aspects are the possibility to integrate all laboratory tasks on a small chip and the advantages of using fluidic systems that scale down by a factor of 1000 or more compared to standard laboratory setups. Because of this extreme size reduction, only minute quantities of sample and reagents are necessary for a lab-on-a-chip system. Instead of dealing with 1 L or 1 mL, a microfluidic device may be efficiently operating with 1 nL or 1 pL of fluids [2]. The benefits of operating with such small volumes are fast reaction times and the possibility to make an analysis even if only small amount of sample are available [3].

Furthermore, magnetic microparticles and nanoparticles have gained significant interest worldwide and are being used in bioanalysis for many applications [1]. Magnetic particles (MPs) can be manipulated inside microfluidic channels by establishing magnetic fields, either with permanent magnets or electromagnets. These magnets can be outside the microfluidic channel and, therefore, do not need to be in contact with the sample solution [4]. To exert a translational force on MPs and, therefore, be able to transport them, a magnetic field gradient is required. This movement of suspended MPs in a microfluidic channel under the influence of a magnetic field is called magnetophoresis. Secondly, micro- and nanoparticles offer a relatively large surface in relation to their volume. This surface can be modified so as to chemically bind to a specific analyte [3]. Hence, this functionalization, in combination with the possibility of magnetic manipulation, allows then to indirectly control biomolecules attached to the MPs [5]. Thirdly, MPs can be detected by integrated magnetic field sensors, offering a compact and integrated solution with high sensitivity and reliability.

This thesis is part of a three year project which started in September 2012 and is sponsored by the FWF - Fonds zur Förderung der wissenschaftlichen Forschung, project number P24372-N19. The goal of the project is to develop a biosensing system that detects a non-magnetic analyte by utilizing the motion of MPs suspended in a microfluidic channel. MPs that are attracted by a magnetic force will reach a certain velocity inside the microfluidic channel. If the same MPs are covered with a layer of non-magnetic analyte due to their functionalization (called loaded MPs or LMPs), their overall volume increases while their magnetic volume

remains the same. While experiencing the same attractive magnetic forces as the bare MPs, the drag force, which opposes the magnetic force, will increase for the LMPs and, therefore, their velocity will decrease. This velocity change caused by volumetric change can be used to discriminate between MPs and LMPs. LMPs need more time to travel through the microchannel than bare MPs. The needed magnetic field gradient was generated by current carrying conductors which are actuated by a microcontroller. In the course of this thesis the MP movement, hence the time the MPs need to travel through the channel, was monitored by an optical microscope, whereas later in the project the movement will be detected by magnetic field microsensors located near the channel inlet and outlet. The goal of this thesis is to produce a first prototype of the biosensing device and then use this device to prove the concept of the detection method which utilizes volumetric change as a cause for velocity change.

The next chapter provides a theoretical background on magnetophoresis, gives examples of current work in the field of magnetic biosensors and depicts the advantages of the proposed method. Chapter 3 deals with the design of the biosensing system and its implementation. Calculations are presented concerning the velocity change caused by the volume change of MPs, and concerning the magnetic field generated by rectangular conductors. Design requirements and considerations are discussed and FEM (finite element method) simulations of various geometries for the conductors and various MPs, in order to determine the optimum parameters for the system, are reported. In chapter 4 the fabrication of the chip and the measuring set-up are described and the results of the measurements are presented. Finally, in chapter 5, the results are discussed and an outlook on the further development of the project is given.

2 Theory

In this chapter magnetophoresis, the method on which the biosensing system described in this thesis relies, is explained (section 2.1). Relevant microfluidic terms are defined and the fundamentals of magnetic particles (MPs) and the forces which act on them are described. In section 2.2 existing state of the art magnetic biosensors are presented and the advantages of the proposed method are illustrated.

2.1 Magnetophoresis

Magnetophoresis is the movement of magnetic particles dispersed in a buffer fluid under the influence of a magnetic field [6]. Specifically, the MP containing fluid is introduced into a microfluidic channel. The magnetic force F_m acting on the MPs and, therefore, their movement is proportional to the magnitude of the magnetic flux density B, the gradient of the magnetic field $\nabla \cdot B$, the particle volume V_P and the difference in magnetic susceptibility between the fluid and the MPs $\Delta\chi$ (see equation (2.7)). The MPs can be functionalized by coating them with ligands, which have a specific affinity to a nonmagnetic analyte. Using this specific binding, the movement of MPs can be used to detect or to capture the analyte in the fluid.

2.1.1 Laminar vs. turbulent flow

The laminar or turbulent flow in long straight channels of constant cross section is predicted by the Reynolds number (*Re*) which is given by:

$$Re = \frac{\rho D_h u}{\eta} \tag{2.1}$$

where ρ is the density of the fluid, D_h is the hydraulic diameter, u is the characteristic velocity of the fluid in the channel and η is the dynamic viscosity of the fluid. From a physical point of view, the Reynolds number describes the ratio between inertial forces and viscous forces in a

particular flow. For *Re* << 1 viscous effects dominate inertial effects, for *Re* ≈ 1 viscous effects are comparable to inertial effects and for *Re* >> 1 inertial effects dominate viscous effects [7].

The hydraulic diameter D_h takes the shape of the channel into consideration and is used if the shape is other than circular. It is given by:

$$D_h = \frac{4\ x\ Cross\ Section\ Area}{Wetted\ Perimeter} = \frac{4A}{P_{Wet}} \tag{2.2}$$

where *A* is the area of the channel through which the fluid is flowing and P_{Wet} refers to the perimeter of the channel that is in direct contact to the fluid. This means that the hydraulic diameter can be used to describe completely filled channels as well as only partially filled ones. For a completely filled channel, *A* is simply the area of the channel and P_{Wet} its perimeter [7].

The transition from laminar to turbulent flow occurs typically in the range of *Re* = 1000 to 2000 and is a function of several parameters such as the channel shape, aspect ratio and surface roughness [7]. Figure 2.1 illustrates the respective flow profile of laminar and turbulent flow. Since in microfluidics *Re* is normally << 1, the flow is highly laminar.

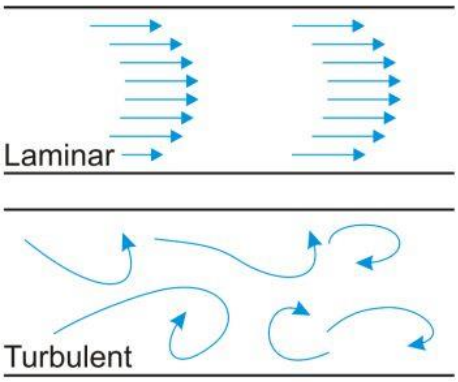

Figure 2.1: Flow profile of laminar and turbulent flow [8]

2.1.2 Fundamentals of magnetic particles

The magnetization curve (magnetization *M* as a function of the magnetic field *H*) of a material can be used to describe its magnetic behavior. Figure 2.2 illustrates a magnetization curve of a ferromagnetic material showing the typical hysteresis loop. As the external magnetic field increases, the spins in the material will at some point all align with the external magnetic field and the magnetization of the material reaches its maximum value, the saturation

magnetization M_s. When the applied magnetic field decreases, the spins will cease to be aligned with the field, hence the total magnetization of the material decreases. When the external magnetic field decreases to zero, a ferromagnetic material retains a considerable degree of magnetization, called remanent magnetization M_r. To bring the magnetization of the material back to zero, a magnetic field in the negative direction has to be applied. The value of the external field at which the magnetization becomes zero is called coercive field, H_c. If the field is further increased in the negative direction, the material reaches at some point its saturation magnetization in negative direction. When the external field decreases, reaches zero, and is increased in positive direction, the hysteresis loop is completed [9].

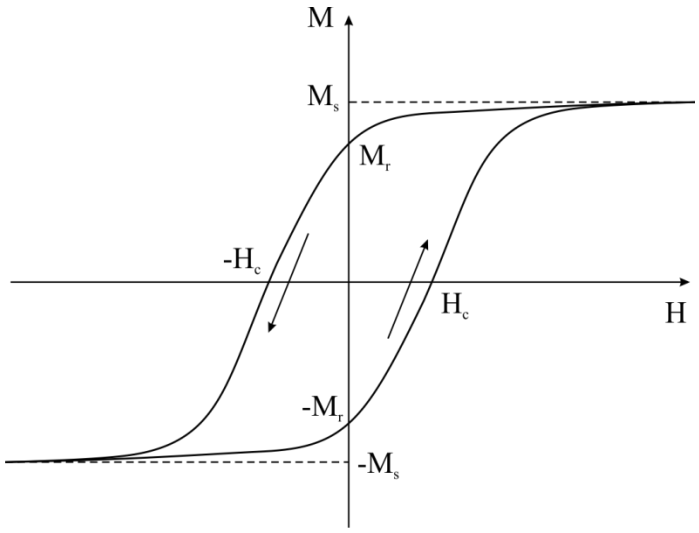

Figure 2.2: Typical magnetization curve (magnetization M as a function of the magnetic field H) of a ferromagnetic material showing hysteresis. Several magnetic parameters are shown: saturation magnetization M_s, remanent magnetization M_r, and coercitivity H_c

All materials react to magnetic fields to some extent. They can be classified by their volumetric magnetic susceptibility χ, which describes the relation between the magnetization M induced in a material by the magnetic field H:

$$M = \chi H \tag{2.3}$$

Most materials display little magnetism in the presence of an external field. These materials are classified either as paramagnets (χ = 10^{-6} to 10^{-1}), or diamagnets (χ = -10^{-6} to -10^{-3}). However, some materials exhibit ordered magnetic states and are magnetic even without a field applied; these are classified as ferromagnets, ferrimagnets and antiferromagnets, where the prefix refers to the nature of the coupling interaction between the electrons within the material [9]. Large spontaneous magnetizations may arise because of this coupling, which leads to much larger χ and M values. The susceptibility in ordered materials depends on the applied magnetic field, which is the reason for the characteristic sigmoidal shape of the

magnetization curve, with *M* reaching a saturation value at high values of *H*. Hysteresis loops can be observed in ferromagnetic and ferrimagnetic materials [9] (see Figure 2.2).

A group of spins with the same direction of magnetic moments that act cooperatively in the magnetization procedure is called a domain. Domains are separated by domain walls, which have a characteristic width and energy associated with their formation and existence. Domain wall movement is a primary means of reversing magnetization. Figure 2.3 qualitatively shows the relation between the coercitivity and particle sizes in particle systems [10]. In large particles (micron sized or even bigger), energetic considerations favor the formation of domain walls, thus giving rise to a multi-domain structure. The magnetization of such particles is realized by domain wall movement. As the particle size decreases and approaches a critical particle diameter, D_c, the formation of domain walls becomes energetically unfavorable and the particles consist of single-domains. Magnetization changes in single-domain particles are realized through the rotation of magnetic domains. As the particle size is much smaller than D_c, the spins in the particles are affected by thermal fluctuations and such particles are called superparamagnetic particles [10]. The magnetization curve of superparamagnetic particles is anhysteretic, but still sigmoidal [9]. This means that they show no remanent magnetization after removal of an external magnetic field, and it is possible to "turn off" the magnetization of superparamagnetic particles by removing the magnetic field. Figure 2.4 illustrates magnetization curves for diamagnetic, paramagnetic, and superparamagnetic materials.

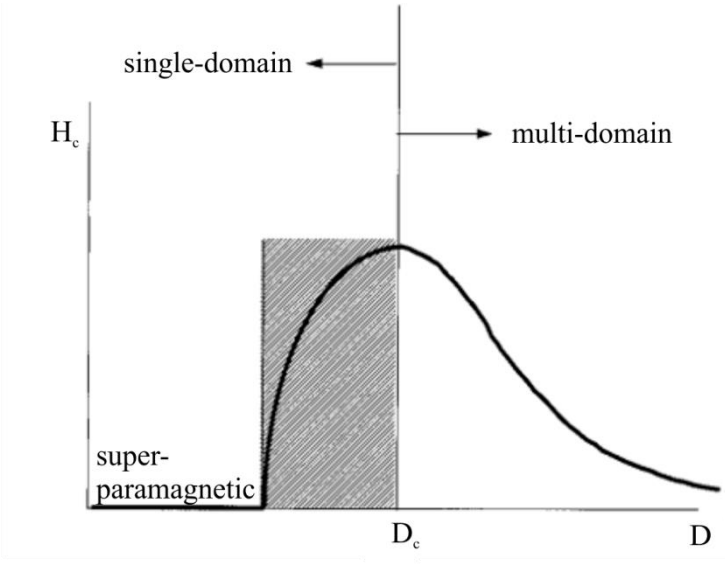

Figure 2.3: Relation between the coercitivity and particle sizes in particle systems [10]

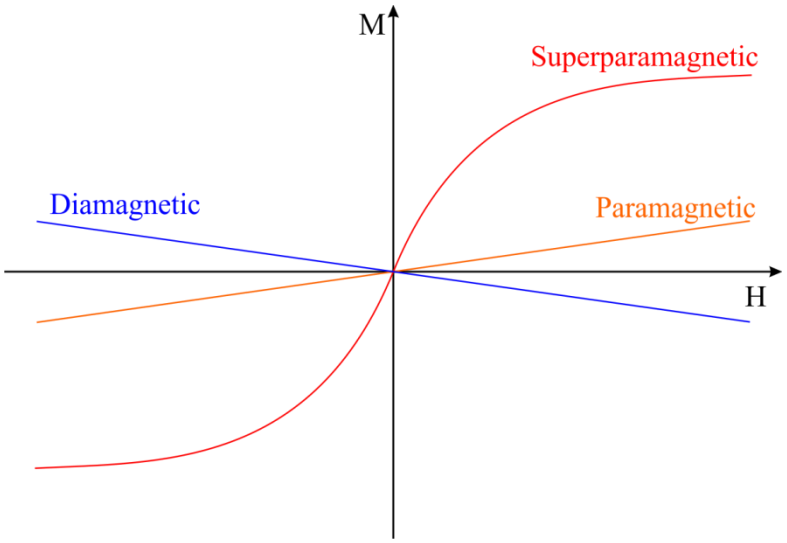

Figure 2.4: Magnetization curves for diamagnetic, paramagnetic, and superparamagnetic materials

2.1.3 Forces acting on magnetic particles

Magnetic force

A single MP can be approximated by a point like magnetic dipole which has a magnetic moment

$$\vec{m} = V_P \vec{M} \tag{2.4}$$

where V_P is the particle volume, and $\vec{M}$ is the magnetization. In the case of a superparamagnetic microparticle the magnetization can be written as

$$\vec{M} = \Delta\chi \vec{H} \tag{2.5}$$

where $\Delta\chi = \chi_P - \chi_{fluid}$ is the volumetric magnetic susceptibility difference between the particle (χ_P) and the surrounding fluid (χ_{fluid}) and $\vec{H}$ is the magnetic field. The magnetic force experienced by the superparamagnetic MP is given by

$$\overrightarrow{F_m} = (\vec{m} \cdot \nabla)\, \vec{B} \tag{2.6}$$

where $\nabla \cdot \vec{B}$ is the gradient of the magnetic field. When combining equations (2.4) to (2.6) and using the relation $\vec{B} = \mu_0 \vec{H}$, it becomes apparent that the magnetic force acting on the superparamagnetic MP is proportional to the magnetic flux density $\vec{B}$, the gradient of the magnetic field $\nabla \cdot \vec{B}$, the particle volume V_P and the difference in magnetic susceptibility between the fluid and the MP $\Delta\chi$ [1], [11]. It is given by equation (2.7):

$$\overrightarrow{F_m} = \frac{V_P \Delta\chi}{\mu_0}\left(\vec{B}\cdot\nabla\right)\vec{B} \tag{2.7}$$

Assuming that there are no time-varying electric fields or currents, the Maxwell equation $\nabla \times \vec{B} = 0$ can be used [9]. If this equation is applied to the mathematical identity

$$\nabla\left(\vec{B}\cdot\vec{B}\right) = 2\left(\vec{B}\cdot\nabla\right)\vec{B} + 2\vec{B}\times\left(\nabla\times\vec{B}\right) \tag{2.8}$$

the following identity is obtained:

$$\frac{1}{2}\nabla\left(\vec{B}\cdot\vec{B}\right) = \left(\vec{B}\cdot\nabla\right)\vec{B} \tag{2.9}$$

and equation (2.7) can be written as:

$$\overrightarrow{F_m} = \frac{V_P \Delta\chi}{2\mu_0}\vec{\nabla}\,\vec{B}^2 \tag{2.10}$$

Drag force

Opposing the magnetic force F_m, the drag force F_d is acting on the MP. Assuming laminar flow in the microfluidic channel and the particle being spherical, Stokes's law can be used to determine F_d. It is proportional to the radius r of the MP and a consequence of the velocity difference $\Delta u = u_P - u_{fluid}$ between the MP (u_P) and the fluid (u_{fluid}). For a spherical MP with radius r the drag force is given by

$$\overrightarrow{F_d} = 6\pi\eta r\Delta\mathrm{u} \tag{2.11}$$

DLVO force

Electrostatic and electrodynamic (Van der Waals) forces are commonly referred to as DLVO forces, named after the scientists that first described them in detail (Derjaguin, Landav, Verwey, Overbeek). According to [12] a layer of SiO_2 produces a negatively charged surface in aqueous buffer, thus producing a repulsive force between negatively charged particles and the solid surface. In consequence this DLVO force is a counterforce to the y-component of the magnetophoretic force F_m and can be used to avoid particle-solid surface adhesion.

The described forces acting on the MP are illustrated in Figure 2.5 in the case of a permanent magnet as the source of the magnetic force.

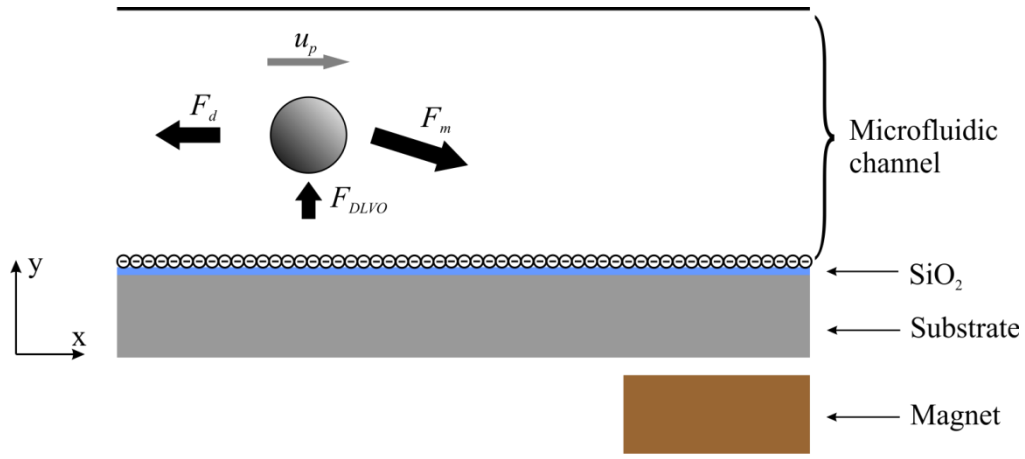

Figure 2.5: Forces experienced by a magnetic particle in a microfluidic channel, with an SiO_2 layer on the substrate and a permanent magnet as the source of the magnetic force: The drag force F_d, the magnetic force F_m and the DLVO Force F_{DLVO}. Also shown: the resulting particle velocity u_p

2.1.4 Magnetic field

As noted above, a single MP can be approximated by a point like magnetic dipole. Upon the application of a uniform magnetic field such a dipole experiences a torque, but no translational action (see Figure 2.6 (a) and (b)). To be able to transport MPs using a magnetic field, a magnetic field gradient is required which will exert a translational force (see Figure 2.6 (c)). Magnetic field gradients are determined by the rate of change of the strength of the field over distance [13].

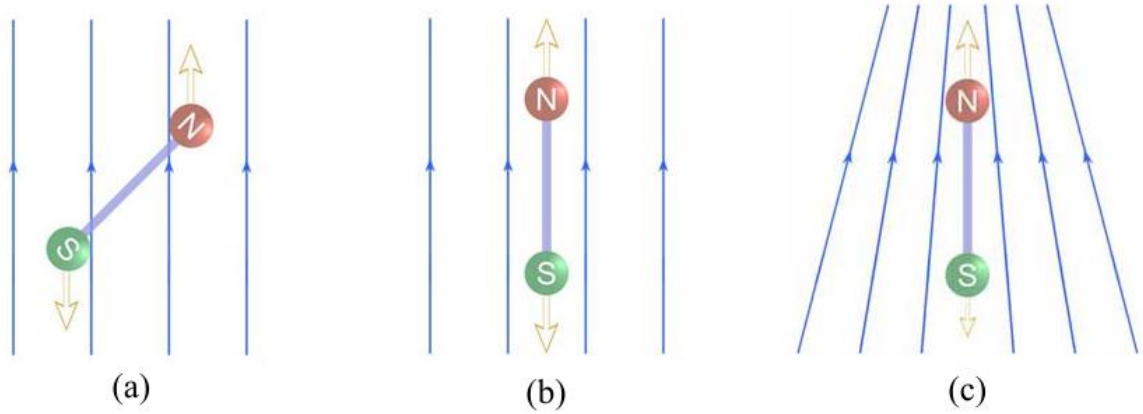

Figure 2.6: A uniform field does not exert translational force on a dipole (a), it just tends to orient a magnetic dipole until forces on the north and south pole balance (b). To exert a translational force on a dipole a field gradient is required (c), the figure shows stronger force on the north pole than the south pole [13].

One way to generate the needed magnetic field gradient is to use external permanent magnets, their advantage being the high magnetic induction that they generate. However, external magnets cannot be easily miniaturized and controlling their magnetic field is challenging. If

size or field control is an issue for a given application, electromagnets can be used to generate the field gradient; in the simplest form consisting only of current carrying electrical conductors. The magnetic field of a straight, very long, filamentary conductor is given by:

$$B = \frac{\mu_0 I}{2\pi r} \tag{2.12}$$

where, I is the current flowing through the conductor, μ_0 is the permeability in vacuum and r is the distance from the conductor at which the magnetic flux density B is calculated. Equation (2.12) shows that the magnetic field of such a conductor declines with $1/r$ over distance, thus establishing the required magnetic field gradient. In the biosensing system presented in this thesis rectangular conductors are used; the corresponding field generated by these conductors is calculated in section 3.2.2.

2.2 Magnetic Biosensors: state of the art

Hoshino et al. describe in [14] a system to separate and detect tumor cells in a sample of blood. Figure 2.7 shows an illustration of the system. The blood sample, containing cultured carcinoma cells, is combined with MPs which are functionalized to attach to the cancer cells. The cancer cells then bind to the MPs and are collected by permanent magnets as the blood is pumped through a microchannel placed on top of the magnets.

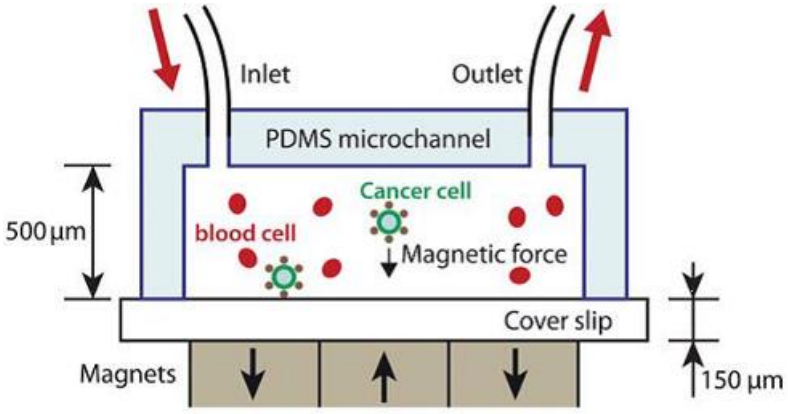

Figure 2.7: Illustration of the system described in [14]. Cancer cells in blood are labeled with functionalized MPs, and captured by the magnetic field as the blood flows through the microchannel.

The bottom glass coverslip is detached from the PDMS (polydimethylsiloxane) microchannel after screening the blood sample and serves as a slide for microscope observation. An array of three alternately arranged magnets with opposite polarities next to each other is used to yield a large magnetic field gradient

As a first step in the screening process the microchannel is filled with PBS (phosphate buffered saline) to eject air bubbles, then the cancer cells containing solution is driven pneumatically at a continuous rate and the magnetically labeled cancer cells are immobilized by the magnet array. To remove unwanted blood cells from the bottom glass slide PBS is introduced in a next step and flowed continuously until the red blood cells are not visible in the channel. Then 1 mL of icecold acetone is introduced to the microchannel to fix the cancer cells onto the glass slide. Finally, after the bottom glass coverslip is being disassembled and dried, the cells are fluorescently stained for observation. Figure 2.8 shows a photograph of the experimental setup.

One disadvantage of this system is the limited possibility of miniaturization because external permanent magnets are used. Another disadvantage is that in order to perform a measurement, several steps have to be carried out, including the disassembling of the device and the need to fluorescently stain the cells.

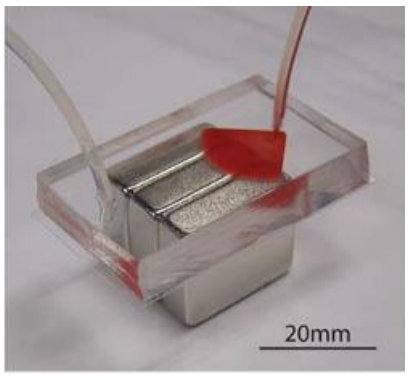

Figure 2.8: Photograph of the experimental setup of the system described in [14]. A blood sample is being introduced into the microchannel

In [15] L. A. Sasso et al. present a microfluidic device that automatically performs the serial processing steps of an antigen sandwich immunoassay to directly measure protein concentrations in an unmodified sample stream.

Magnets are placed on both sides of a microchannel to attract MPs and enable the incubation with antigens and fluorescent antibody markers along the walls of the channel. The MPs progress transversely across the channel to enter or exit reactant streams. Coplanar flow environments from multiple converging inlets are established: a particle carrier stream, antigen containing stream and wash stream. By placing magnets on opposite sidewalls, the MPs can be pulled into and out of the different streams and the incubation time can be adjusted by changing the flow rate. At the channel end fluorescence detection on a microscopy platform takes place. Figure 2.9 illustrates the principle. “Magnet 1” pulls the MPs into the antigen sample stream (biotin-FITC (fluorescein isothiocyanate)) where they roll along the sidewall while incubation occurs. “Magnet 2” pulls them out of the sample stream and into a wash stream, followed by fluorescence detection.

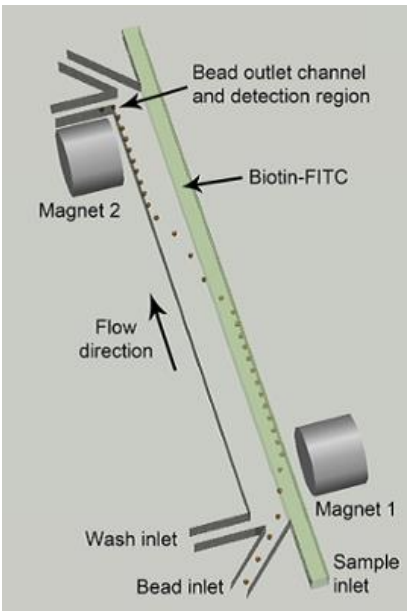

Figure 2.9: Illustration of working principle of the microfluidic system described in [15]. "Magnet 1" pulls the MPs into the antigen sample stream (biotin-FITC) and "Magnet 2" pulls them out of the sample stream and into a wash stream, followed by fluorescence detection.

Additionaly a dual incubation version was developed that added a second cycle of this scheme after the first incubation. This enables a primary incubation of antibody-coated MPs with an untagged antigen, followed by a secondary incubation of the antigen-coated MPs with a fluorescently tagged secondary antibody (Figure 2.10).

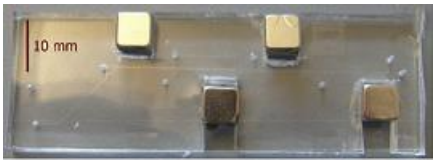

Figure 2.10: Photograph of the dual incubation device described in [15] with several inlets and outlets for the incubation and washing stages.

The disadvantages of this system are the usage of external permanent magnets, which limits the miniaturization, and the need of a microscope to detect the fluorescently tagged proteins.

In [16] Dittmer et al. present a biosensor system to detect cardiac troponin I (cTnI) in a finger-prick blood sample. The system incorporates MPs and electromagnets to control all occurring reaction processes. The optical technique of frustrated total internal reflection is used as detection method.

The cTnI test is a one-step sandwich immunoassay occurring in a stationary liquid in a reaction chamber. Electromagnets, consisting of copper coils which were wound around a 2.5

mm cobalt–iron alloy core, positioned on top and bottom of the chamber are used to control all assay processes (Figure 2.11). The bottom surface of the reaction chamber is functionalized with capture antibodies and serves as the sensing surface.

First, antibody loaded MPs move through the solution for effective analyte capture (Figure 2.11 (a)). Then the bottom electromagnet is used to transport the particles to the sensor surface for binding (Figure 2.11 (b)). Finally, the bottom magnet is turned off and the top magnet is turned on to pull the unbound particles away from the sensor surface. The presence of MPs attached to the sensor surface is determined by illuminating the reaction chamber above the critical angle and measuring the decrease in reflected light. The signal of reflected light intensity being higher in the absence of MPs compared to the reflected light intensity during the assay (Figure 2.12).

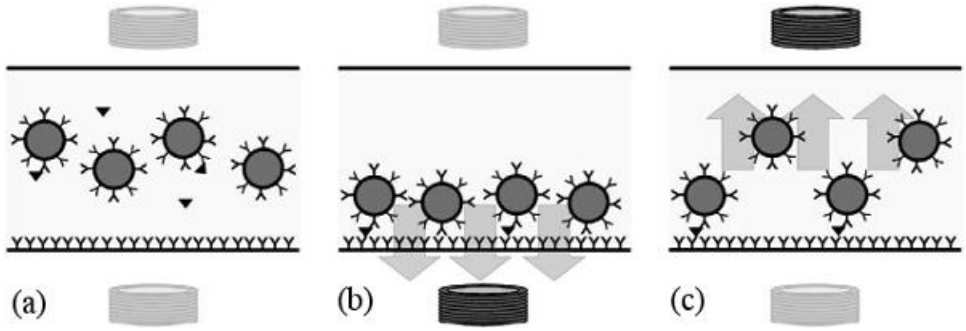

Figure 2.11: Illustration of the reaction chamber and actuation magnets showing successively the assay processes of the system described in [16]: (a) analyte binding by antibody-functionalized MPs (top and bottom magnets off), (b) MP binding to the sensor surface (bottom magnet on) and (c) magnetic removal of free and weakly bound MPs (top magnet on)

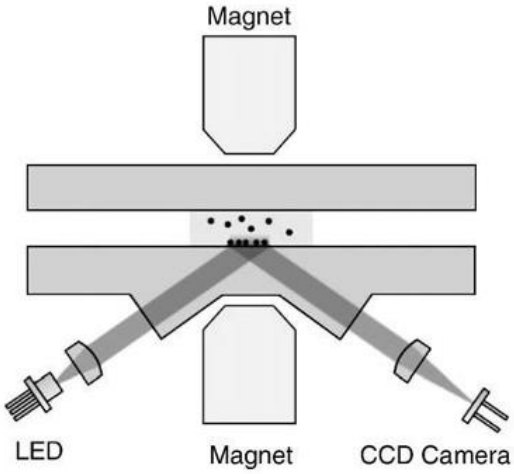

Figure 2.12: Schematic of the system described in [16] consisting of the top and bottom magnets and the detection optics. The presence of MPs attached to the sensor surface is determined by illuminating the reaction chamber above the critical angle and measuring the decrease in reflected light.

The major disadvantage of this system is that the bottom surface of the reaction chamber needs to be functionalized with capture antibodies. This biological functionalization is prone to time dependent changes such as aging and contamination.

In comparison to the presented systems the biosensing system presented in this work has the following advantages:

- No need for big external permanent magnets which would limit miniaturization (as are used in [14] and [15]). Instead current carrying microstructures are used to generate the magnetic field gradient.
- Additionally this allows a controlled manipulation, concentration or separation of the MPs.
- Access to the bioanalyte in the whole fluid sample as compared to other techniques (as proposed in [16]), which have access only to bioanalyte, which is in contact with a functionalized surface.
- No need for a biological functionalization layer (e.g. antibodies, proteins) as mentioned in [16] which is prone to time dependent changes such as aging and contamination. Long-term stability is an issue with biosensors which depend on such a layer. This is not the case with the proposed biosensing device since it is based on functionalized MPs that will be refreshed for every measurement.
- The extra step of adding fluorescent particles to the MPs, as proposed in [14] and [15] can be avoided. Additionally, existing on-chip detection devices which use fluorescent detection in order to measure the velocity of the accelerated MPs need either optical microscopes or CCD cameras to utilize the detection. As already mentioned in the Introduction, this thesis is part of a project that will continue after the work presented here. Later on in the project magnetic detection will be investigated as an alternative detection principle. This can be realized by magnetic field sensors (e.g. giant magneto resistance (GMR) microsensors) placed near the inlet and the outlet of the microfluidic channels. When MPs are introduced into the microchannel the first field sensor registers a change in its electrical resistance, and when they exit the channel the second sensor does. If the time difference between the detection of the resistance change on the first sensor and the detection of the resistance change on the second sensor is measured, the particle velocity can be calculated.

3 System Design and Implementation

In this chapter the design of the biosensing system and its implementation are being described. Specifically, section 3.1 presents the working principle of the system which is based on the velocity change of MPs while being accelerated by a translational magnetic force due to a change in their volume by the presence of analyte. In section 3.2 calculations are reported, concerning the change in velocity when the volume of MPs changes, and concerning the magnetic field generated by rectangular conductors. The magnetic field simulations using COMSOL Multiphysics, a finite element analysis, solver and simulation software are also reported as well as the comparison between simulations and calculations in order to verify the result of the simulation software. Section 3.3 describes the design of the system and section 3.4 the simulations (using COMSOL) of various geometries for the conductors and various MPs, in order to find the optimum parameters for the system.

3.1 Working principle

The purpose of the biosensing system presented in this work is to detect specific nonmagnetic analyte, e.g. cells or viruses. Therefore MPs, with a given radius r and volume V, are functionalized by coating them with ligands, which have a specific affinity to the nonmagnetic analyte. Then they are mixed with the sample fluid under investigation which either does or does not contain the analyte. If the fluid contains the analyte of radius r_a, the analyte binds to the coated MPs, therefore forming new compounds. These compounds are called loaded magnetic microparticles (LMPs) and they have a total radius r' and a total volume V' (see Figure 3.1).

The LMP containing fluid is then introduced into a microfluidic channel which is called the measurement channel. In a second reference channel the sample fluid containing uncoated, and thus unloaded, MPs is also being introduced. Under the influence of an external magnetic field generated by electrical conductors, MPs and LMPs experience the same attractive forces. However, because of the difference in volume they will gain different velocities; with increasing volume, due to the attached (nonmagnetic) analyte, the drag force increases in the opposite direction to that of the magnetic force. Hence, the difference in velocities, which is translated into a difference of the time MPs and LMPs need to travel a certain distance,

determines the presence of analyte in the fluid under investigation. In particular, even though the LMPs in the measurement channel and the MPs in the reference channel have the same magnetic volume the overall volume of the LMPs is bigger than that of the MPs. Thus the LMPs need more time to travel the same distance than the MPs [1].

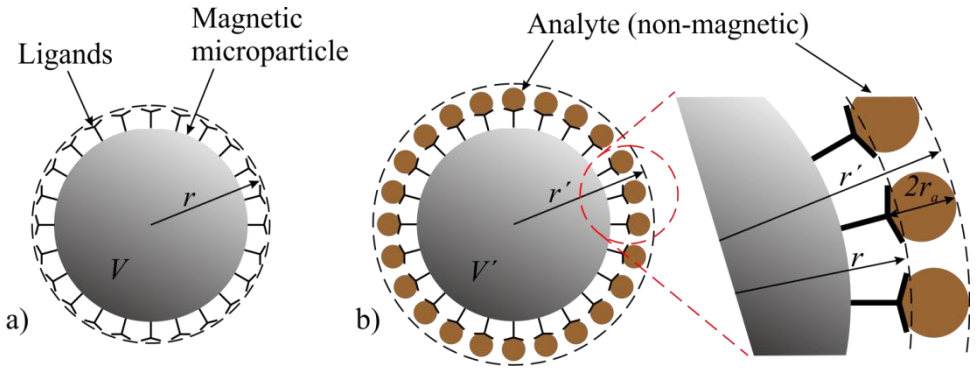

Figure 3.1: (a) Magnetic microparticle (MP) coated with ligands, having a total radius *r* and total volume *V* and (b) loaded magnetic microparticle (LMP) coated with ligands and attached analyte of radius r_a, having of total radius *r'* and total volume *V'*.

3.2 Calculations

3.2.1 Volumetric change

Assuming the magnetic susceptibility of the surrounding medium is zero, the volumetric magnetic susceptibility difference $\Delta\chi$, between the particle (χ_P) and the surrounding fluid (χ_{fluid}) is equal to the susceptibility of the particle χ_P. Therefore the magnetic force experienced by the superparamagnetic MP as given in equation (2.10) can be written as:

$$\overrightarrow{F_m} = \frac{V_P \chi_P}{2\mu_0} \vec{\nabla} \vec{B}^2 \tag{3.1}$$

Since in the described biosensing system the fluid is static, the velocity difference Δu between the MP and the fluid is equal to the velocity of the microparticle u_p. Therefore the drag force for a spherical MP with radius *r*, given by equation (2.11), can be written as:

$$\overrightarrow{F_d} = 6\pi\eta r u_p \tag{3.2}$$

By equating equations (3.1) and (3.2), it is possible to calculate the maximum particle velocity that can be achieved by a magnetic force if the surrounding fluid is static:

$$u_p = \frac{r^2 \chi}{9\mu_0 \eta} \vec{\nabla} \vec{B}^2 \tag{3.3}$$

As previously described the MP will increase in radius if analyte attaches to it, the new radius being $r' \approx r + 2r_a$, where r_a is the radius of the analyte (see Figure 3.1). This increase will only have an influence on the drag force (3.2) and therefore the velocity of the LMP will be given by

$$u'_p = \frac{r^3 \chi}{9\mu_0 \eta r'} \vec{\nabla} \vec{B}^2 \tag{3.4}$$

To determine the decrease in velocity caused by attached analyte equations (3.3) and (3.4) are set into relation in equation (3.5).

$$\frac{u'_p}{u_p} = \frac{r}{r'} \tag{3.5}$$

For MP diameters from 0.5 to 10 µm and analyte diameters from 0.02 to 2 µm this relation is shown in Figure 3.2. It is observed that smaller MPs experience a greater decrease in velocity if loaded with the same analyte than bigger MPs. Therefore, smaller MPs should be favored to establish certain discrimination between LMPs and MPs.

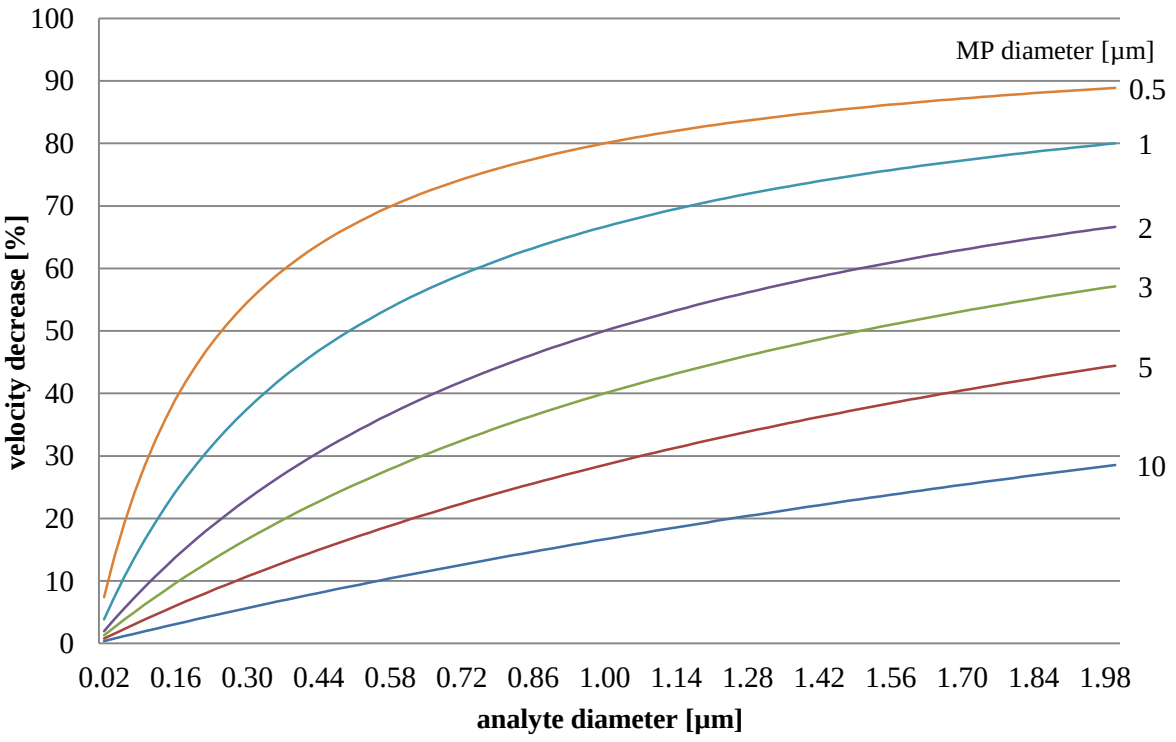

Figure 3.2: Velocity decrease in % of an LMP compared to the unloaded MP in respect to the analyte diameter.

3.2.2 Magnetic field calculations

A given characteristic of filamentary conductors is that the linear dimension of the cross section is much smaller than all the other dimensions, thus the following approximation can be made:

$$j\,\mathrm{d}V \cong js\mathrm{d}l \cong I\mathrm{d}l \tag{3.6}$$

where j is the current density, $I = js$ is the total current flowing in the conductor, and s the cross-sectional area, see Figure 3.3 [17].

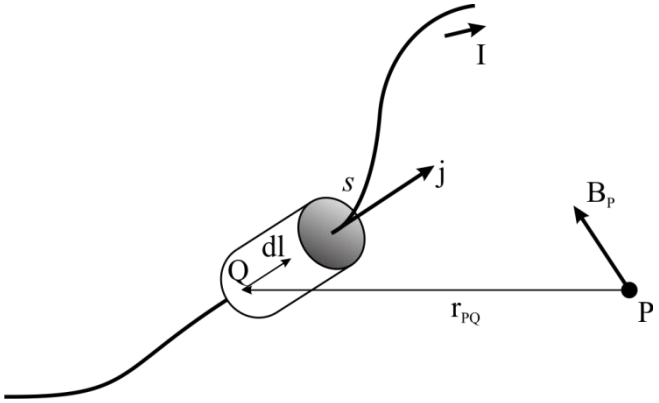

Figure 3.3: Biot-Savart law: magnetic field *B* at point *P* generated by an element (of length d*l*) of a filamentary conductor with a cross-sectional area *s*, running an electric current *I = js*.

To calculate the magnetic field generated by such a current carrying filamentary conductor, the Bio-Savart law is used:

$$B_P = \frac{\mu_0 I}{4\pi}\oint \frac{\mathrm{d}l \times r_{PQ}}{r_{PQ}^3} \tag{3.7}$$

where dl is a vector in the direction of the current and with a magnitude that represents the length of the differential element of the filamentary conductor, and r_{PQ} is the displacement vector from the point at which the field is being calculated to the conductor element, see Figure 3.3

Another way to calculate the field is to determine the vector potential first; for a current carrying filamentary conductor it is given by:

$$A_P = \frac{\mu_0 I}{4\pi}\oint \frac{\mathrm{d}l}{r_{PQ}} \tag{3.8}$$

To calculate the field generated by the very long straight rectangular conductor shown in Figure 3.4 it can be considered as a bundle of filamentary currents, each having a cross section ds and a current jds [18]. The vector potential consists only of the A_z-component; for

each filamentary current of length 2*l* (Figure 3.5) the corresponding contribution dA_z from equation (3.8) can be calculated to

$$\mathrm{d}A_z = \frac{\mu_0}{4\pi} j\mathrm{d}s \int_{-l}^{+l} \frac{\mathrm{d}z}{\sqrt{z^2+r^2}} = \frac{\mu_0}{4\pi} j\mathrm{d}s \ln\left(z+\sqrt{z^2+r^2}\right)_{-l}^{+l} = -\frac{\mu_0}{4\pi} j\mathrm{d}s\left[\ln r - \ln\left(l+\sqrt{l^2+r^2}\right)\right] \quad (3.9)$$

Since $l >> r$, the last term in equation (3.9) becomes independent of *r*, so it does not influence the calculation of the magnetic field $B = \nabla \times A$ and thus can be neglected in the A_z-component:

$$A_z = -\frac{\mu_0}{2\pi}\int j \ln r \mathrm{d}s = -\frac{\mu_0 I}{2\pi S}\int_S \ln r \mathrm{d}s \quad (3.10)$$

The second expression of equation (3.10) with the total current *I* can be used when the current density *j* can be considered as constant over the cross section S of the rectangular conductor.

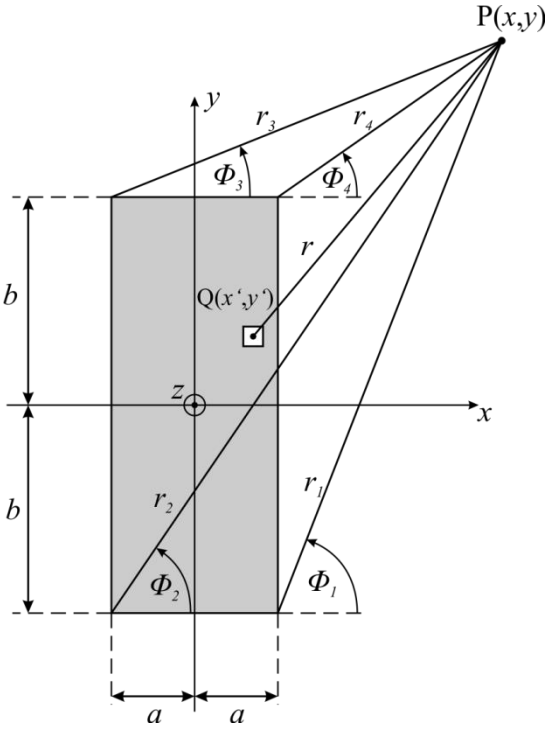

Figure 3.4: Cross section of a rectangular conductor with current flowing uniformingly along the positive z-axis

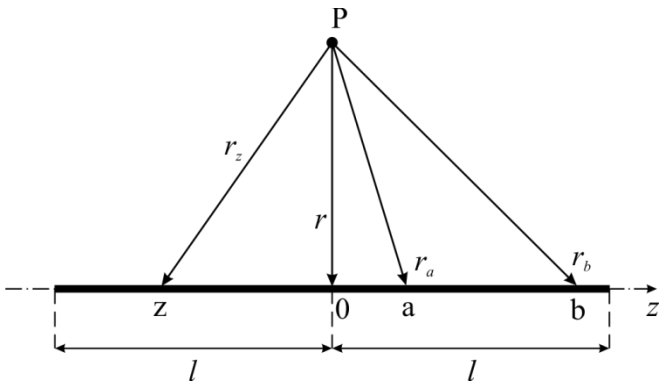

Figure 3.5: Straight, long filamentary current

Using equation (3.10), with $r = \sqrt{(x'-x)^2+(y'-y)^2}$ and $S = 4ab$, the vector potential component A_z for the rectangular straight conductor shown in Figure 3.4 becomes

$$A_z(x,y) = -\frac{\mu_0}{2\pi}\frac{I}{4ab}\int_{-a}^{a}\int_{-b}^{b} \ln\sqrt{(x'-x)^2+(y'-y)^2}\, dx'\, dy' \quad (3.11)$$

Equation (3.11) can be integrated to [18] :

$$A_z = -\frac{\mu_0 I}{16\pi ab}\Big\{(a-x)(b-y)\ln[(a-x)^2+(b-y)^2] + (a+x)(b-y)\ln[(a+x)^2+(b-y)^2] + (a-x)(b+y)\ln[(a-x)^2+(b+y)^2] + (a+x)(b+y)\ln[(a+x)^2+(b+y)^2] + (a-x)^2\left[\tan^{-1}\frac{b-y}{a-x}+\tan^{-1}\frac{b+y}{a-x}\right] + (a+x)^2\left[\tan^{-1}\frac{b-y}{a+x}+\tan^{-1}\frac{b+y}{a+x}\right] + (b-y)^2\left[\tan^{-1}\frac{a-x}{b-y}+\tan^{-1}\frac{a+x}{b-y}\right] + (b+y)^2\left[\tan^{-1}\frac{a-x}{b+y}+\tan^{-1}\frac{a+x}{b+y}\right]\Big\} \quad (3.12)$$

The magnetic field components B_x and B_y are calculated from $B = \nabla \times A$ using the vector relations $(\nabla \times \mathrm{A})_x = \left(\frac{\partial A_z}{\partial y} - \frac{\partial A_y}{\partial z}\right)$ and $(\nabla \times \mathrm{A})_y = \left(\frac{\partial A_x}{\partial z} - \frac{\partial A_z}{\partial x}\right)$:

$$B_x = \frac{\partial A_z}{\partial_y}, \qquad B_y = -\frac{\partial A_z}{\partial_x} \quad (3.13)$$

After differentiation of equation (3.12) as noted in equation (3.13) and using the following definitions (see Figure 3.4):

$$r_1 = \sqrt{[(x-a)^2+(y+b)^2]}, \quad \phi_1 = \tan^{-1}\frac{y+b}{x-a}$$

$$r_2 = \sqrt{[(x+a)^2+(y+b)^2]}, \quad \phi_2 = \tan^{-1}\frac{y+b}{x+a}$$

$$r_3 = \sqrt{[(x+a)^2+(y-b)^2]}, \quad \phi_3 = \tan^{-1}\frac{y-b}{x+a}$$

$$r_4 = \sqrt{[(x-a)^2+(y-b)^2]}, \quad \phi_4 = \tan^{-1}\frac{y-b}{x-a} \quad (3.14)$$

the field components can be written as followed:

$$B_x(x,y) = -\frac{\mu_0 I}{8\pi ab}\left[(y+b)(\phi_1-\phi_2) - (y-b)(\phi_4-\phi_3) + (x+a)\ln\frac{r_2}{r_3} - (x-a)\ln\frac{r_1}{r_4}\right]$$

$$B_y(x,y) = \frac{\mu_0 I}{8\pi ab}\left[(x+a)(\phi_2-\phi_3) - (x-\mathrm{a})(\phi_1-\phi_4) + (\mathrm{y}+\mathrm{b})\ln\frac{r_2}{r_1} - (\mathrm{y}-\mathrm{b})\ln\frac{r_3}{r_4}\right] \quad (3.15)$$

The total amount of the magnetic flux density at coordinates *(x,y)* is given by :

$$B(x,y) = \sqrt{B_x^2 + B_y^2} \quad (3.16)$$

Equations (3.14), (3.15) and (3.16) were used to calculate the magnetic flux density caused by a rectangular conductor with dimensions of $2a$ = 1 µm and $2b$ = 10 µm, running a current of I = 500 mA. The calculations were carried out in MATLAB. The same scenario was also simulated with COMSOL. Then the calculated and the simulated values were compared along three different lines (called cut lines in COMSOL) contiguous to the conductor (see Figure 3.6):

- along the y-axis at the center (x = 0) of the conductor (see Figure 3.7, red cut line in Figure 3.6)
- along the y-axis at the edge (x = 5 µm) of the conductor (see Figure 3.8, black cut line in Figure 3.6)
- along the x-axis at a distance of y = 5 µm from the center of the conductor (see Figure 3.9, green cut line in Figure 3.6)

It can be seen that the values retrieved from the calculation with MATLAB and the simulation are identical, which indicates that the simulation with COMSOL is plausible.

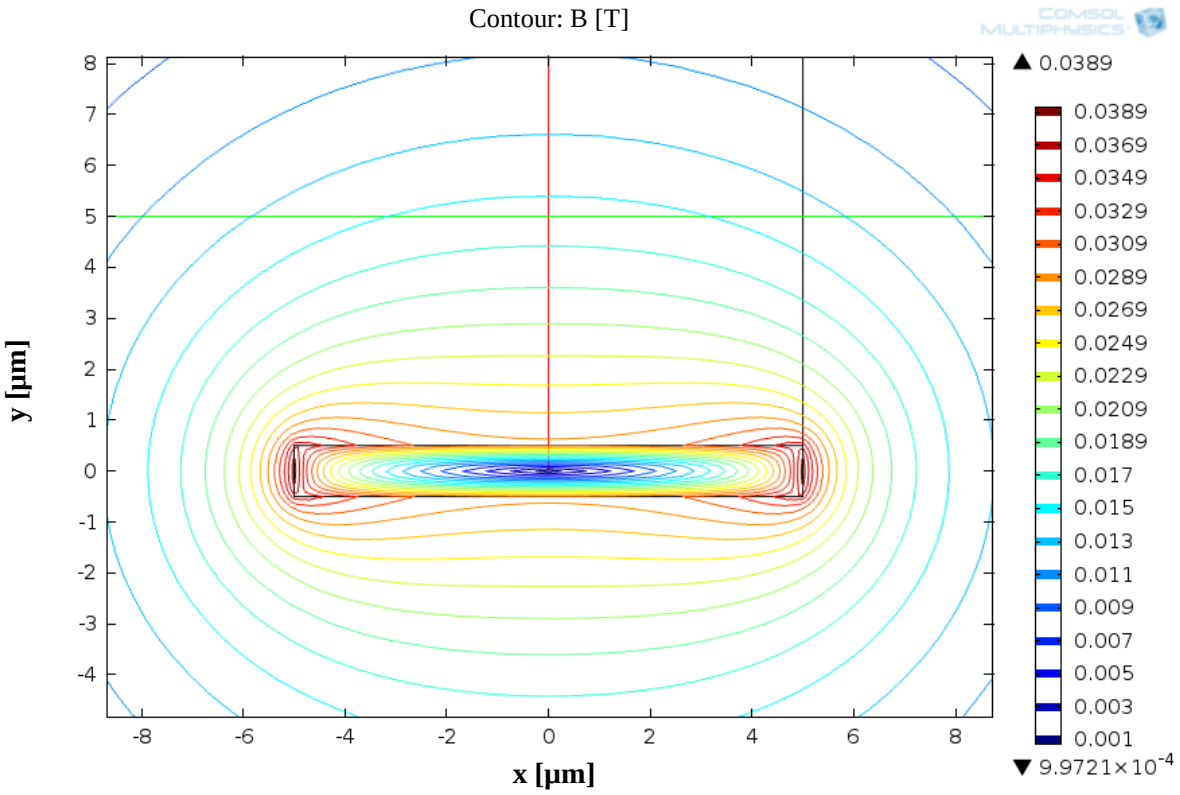

Figure 3.6: Contour plot of the magnetic flux density B caused by a rectangular conductor with dimensions of 1 µm x 10 µm running a current of 500 mA, including cut lines (red, black and green) at which the calculated and simulated values were compared

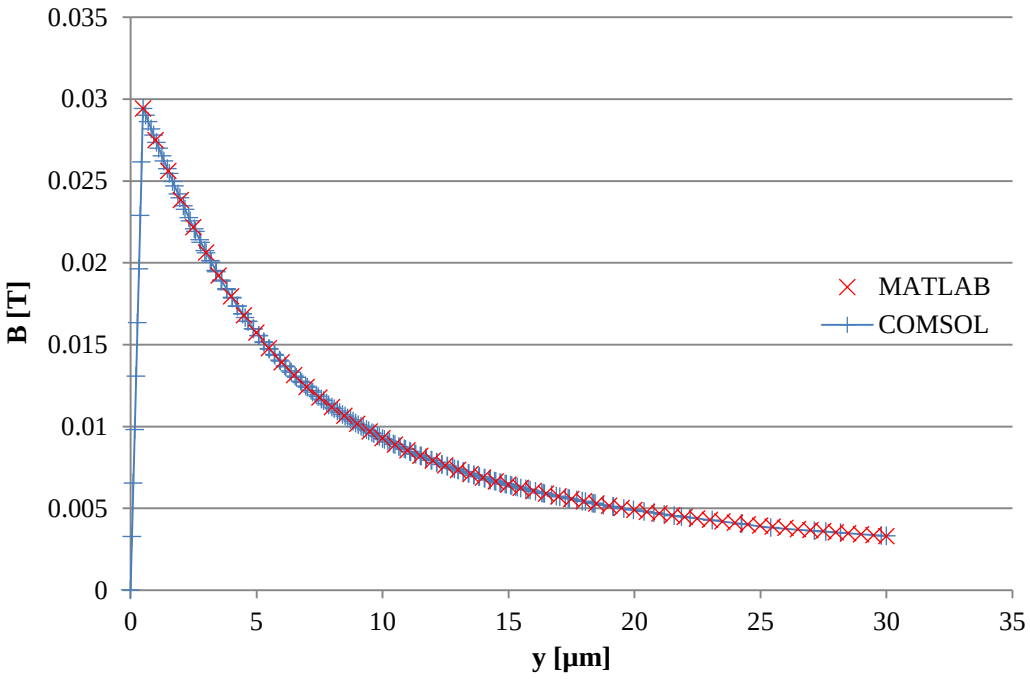

Figure 3.7: Comparison of calculation with MATLAB and simulation with COMSOL of the magnetic flux density along the y-axis at the center of a conductor with dimensions of 1 µm x 10 µm running a current of 500 mA (red cut line in Figure 3.6)

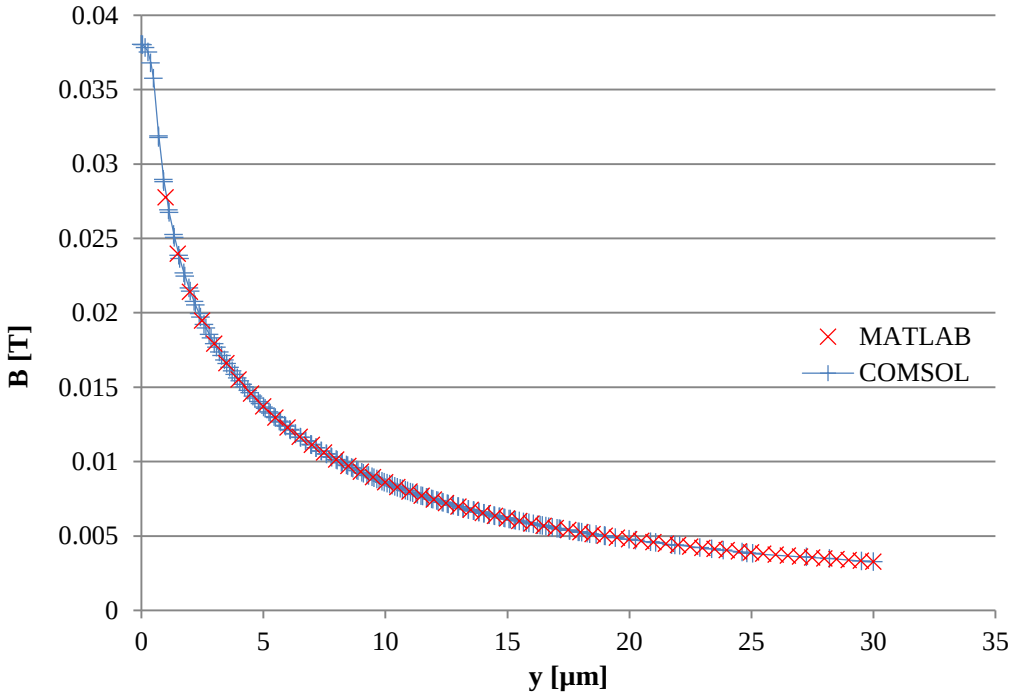

Figure 3.8: Comparison of calculation with MATLAB and simulation with COMSOL of the magnetic flux density along the y-axis at the edge of a conductor with dimensions of 1 µm x 10 µm running a current of 500 mA (black cut line in Figure 3.6)

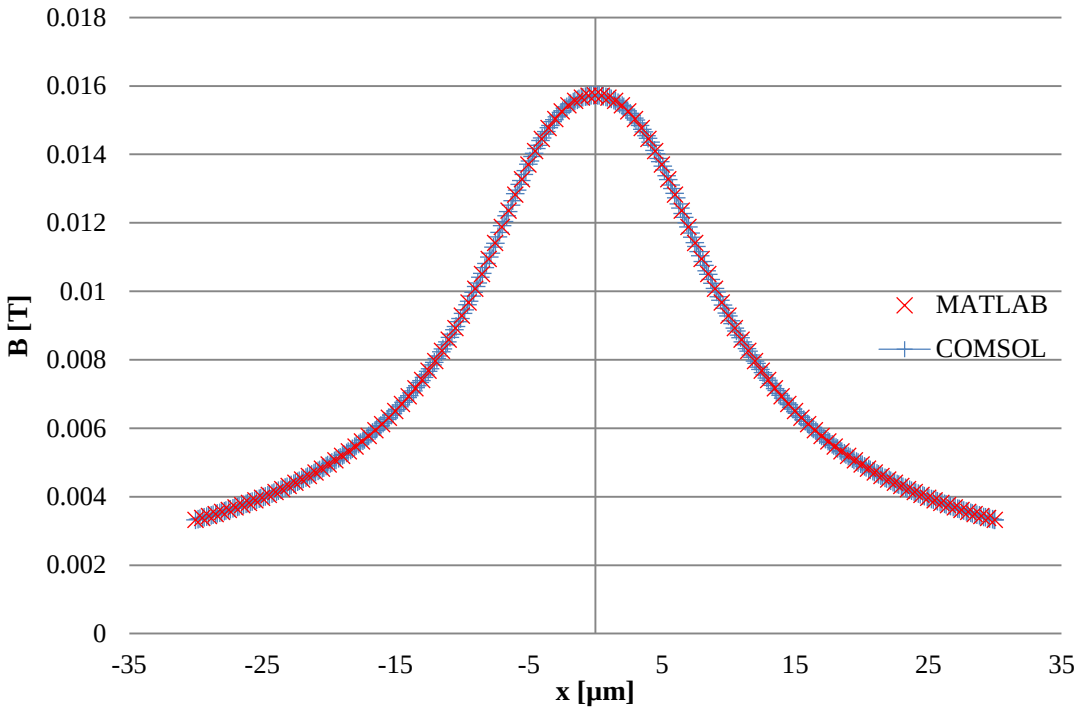

Figure 3.9: Comparison of calculation with MATLAB and simulation with COMSOL of the magnetic flux density along the x-axis at a distance of 5 µm from the center of a conductor with dimensions of 1 µm x 10 µm running a current of 500 mA (green cut line in Figure 3.6)

3.3 Design Requirements and Considerations

The principle design of the biosensing system consists of a microfluidic channel with one inlet and one outlet and below this a layer with current carrying microstructures to establish the needed magnetic field gradient, see Figure 3.10. These microstructures consist of parallel straight rectangular conductors, on which current is sequentially applied. Thus they generate attractive forces on the MPs and therefore induce their movement along the microfluidic channel from the inlet to the outlet. In the course of this thesis the MP movement, hence the time the MPs need to travel through the microchannel, was monitored with an optical microscope (see section 4.4), whereas later in the project the movement is going to be detected by magnetic field microsensors located near the inlet and the outlet.

Several conductor geometries were produced with different conductor widths (c_w) and different distances between the conductors (spacing c_s). Section 3.4 describes simulations that were carried out with COMSOL, to determine which of these geometries is preferable to use. In terms of the current that can be applied to the conductors the joule heating and therefore the current density is the limiting factor. This leaves the conductor thickness (c_{th}) as the last factor that determines the amount of current that can be applied to the different conductor geometries. Two versions were investigated; one with the thickness being 500 nm and the

other with the thickness being 1 µm. In a simulation of the joule heating using conductors with a width of 10 µm and a thickness of 1 µm the maximum applicable current was found to be 200 mA, yielding a current density of $J = 2*10^{10}$ A/m². Table 3.1 lists the different geometries with their respective code-name, conductor width c_w and spacing c_s and the current that is applicable for both conductor thicknesses c_{th}.

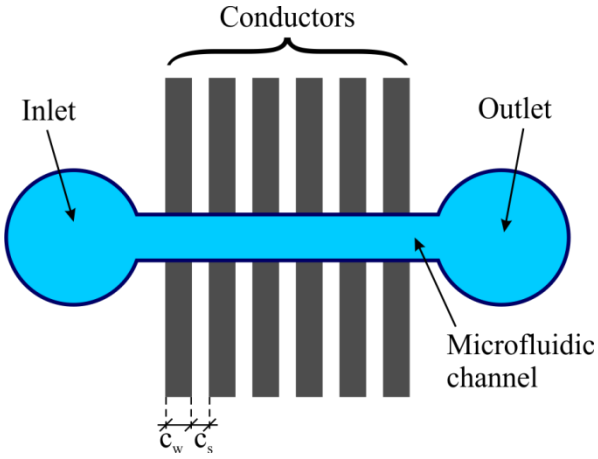

Figure 3.10: Schematic of the biosensing system, consisting of a microfluidic channel with one inlet and one outlet, and current carrying conductors, with conductor width c_w and conductor spacing c_s

code	c_w [µm]	c_s [µm]	current [mA] (c_{th} = 1 µm)	current [mA] (c_{th} = 0.5 µm)
G I	10	8	200	100
G II	10	10	200	100
G III	8	8	160	80
GE I	12	8	240	120
GE II	12	10	240	120
S I	6	5	120	60
S II	6	6	120	60
S III	8	6	160	80
S	4	4	80	40

Table 3.1: Conductor geometries; given are the conductor width c_w and conductor spacing c_s in µm, the respective code-name and the currents in mA that are applicable for the respective conductor thickness c_{th}

In principle an even bigger conductor thickness would be preferable since a bigger conductor cross-section means that the current can be higher, thus yielding a greater magnetic field and therefore also higher attractive forces on the MPs. A simulation was carried out in COMSOL to illustrate this relation, consisting of a rectangular conductor with a width of 10 µm and varying thicknesses from 0.5 to 10 µm. The current density was kept at $J = 2*10^{10}$ A/m² for all these geometries and the magnetic flux density was plotted for a cut line along the x-axis at a distance of 5 µm from the lower border of the conductor. The result is shown in Figure 3.11.

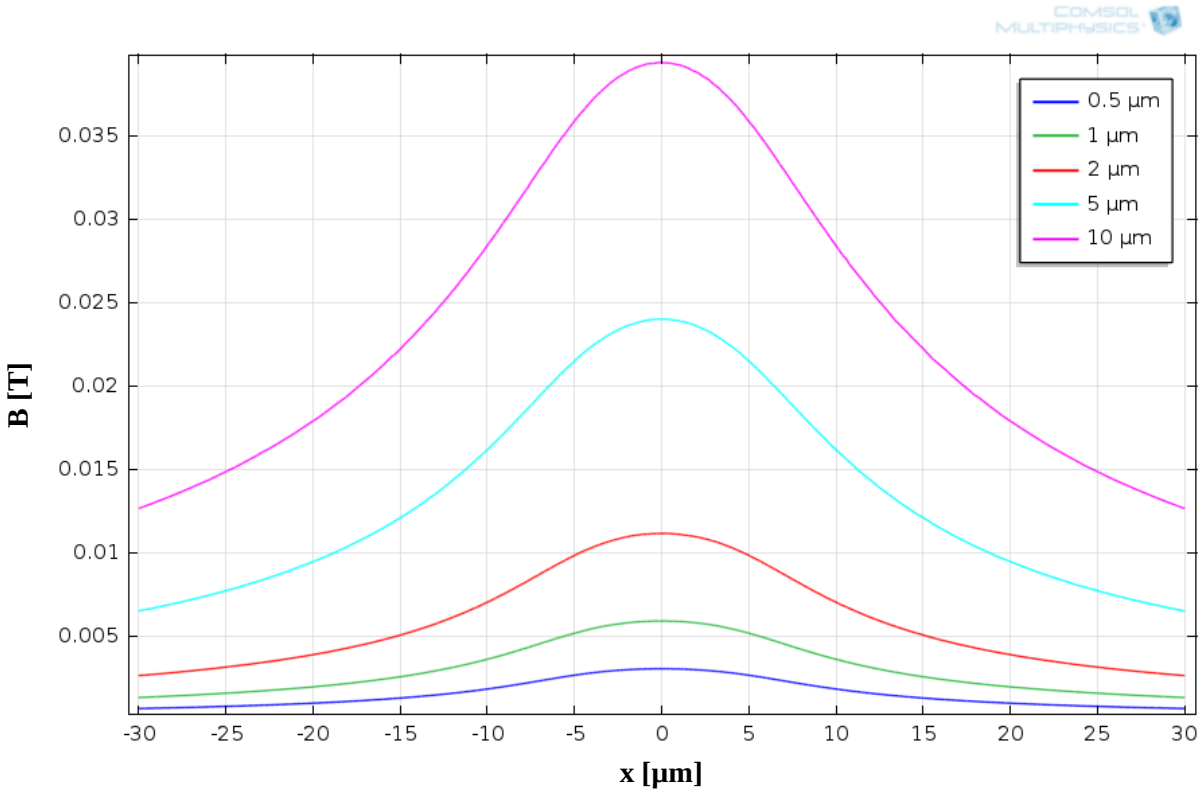

Figure 3.11: Magnetic flux density along the x-axis at a distance of 5 µm from the lower border of a conductor with a width of 10 µm and varying thicknesses (parameter in the plot) and a current density of $J = 2*10^{10}$ A/m²

In practice the maximum achievable conductor thickness is limited because of certain restrictions in the production process; the problem being that the conductors have to be encapsulated in an insulating layer before they can be bonded with the microfluidic channel. Because of the given structure, consisting of parallel conductors separated by certain distances, the insulating layer will not have an even surface; this unevenness getting bigger with the conductor thickness. A conductor thickness of 1 µm was found to be the maximal practicable value.

The geometries with a conductor thickness of 500 nm were insulated by a plasma deposited SiO_2 layer of 500 nm thickness, which has the additional benefit of enabling a repulsive DLVO force between negatively charged particles and the solid surface (see section 2.1.3). In consequence this DLVO force is a counterforce to the y-component of the magnetophoretic force F_m and can be used to avoid particle-solid surface adhesion and the particles getting stuck at the conductor edges; illustrated in Figure 3.12.

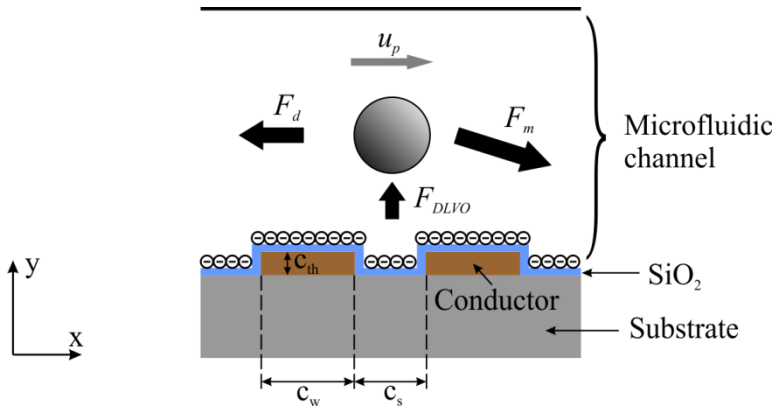

Figure 3.12: Forces experienced by a magnetic particle in the microfluidic channel with SiO_2 insulated conductors, consisting of the drag force F_d, the magnetophoretic force F_m and the DLVO Force F_{DLVO}. Also shown: the resulting particle velocity u_p, conductor width c_w , spacing c_s and thickness c_{th}. (Drawing is not to scale)

For testing and measurement purposes several magnetic MPs were purchased from *micromod Partikeltechnologie GmbH* [19]:

- Pure iron oxide particles consisting of monodisperse magnetite aggregates with a diameter of 250 nm (*iron oxide 250 nm*)
- Magnetic plain silica particles, produced by hydrolysis of orthosilicates in the presence of magnetite, with a mean diameters of 1.5 µm (*sicastar®-M 1.5 µm*)
- Magnetic polystyrene particles; monodisperse particles which consist of magnetite around an organic matrix of a styrene-maleic acid-copolymer and then are coated with a polymer layer for the encapsulation of magnetite and the introduction of chemical functionalities:
    - coated with amino groups and a diameter of 10 µm (*micromer®-M-NH_2 10 µm*)
    - coated with PEG-COOH groups and a diameter of 3 µm (*micromer®-M-PEG-COOH 3 µm*)

In the technical data sheets (see Appendix) the following particle parameters, which are relevant for the project, are given:

- Diameter d in µm
- Density ρ in g/cm³
- Magnetization M in emu/g given for a field of H = 1000 Oe
- Fraction of iron oxide in wt% (given in the safety data sheets[1])

[1] For the sicastar® MPs the fraction of iron oxide is not given in the safety data sheets but was retrieved from an inquiry directed at "micromod Partikeltechnologie GmbH"

The following particle parameters were then calculated from the above mentioned values:

- Volume V in m³ — $V = {}^{1}/_{6}\,\pi d^3$, with d in m
- Density ρ in kg/m³ — $\rho\left[\frac{kg}{m^3}\right] = \rho\left[\frac{g}{cm^3}\right] * 1000$
- Fraction of iron oxide in V% — $V\%_{iron\ oxide} = wt\%_{iron\ oxide}\,\frac{\rho[\frac{kg}{m^3}]}{\rho_{iron\ oxide}[\frac{kg}{m^3}]}$
- Volume of iron oxide in m³ — $V_{iron\ oxide} = V * V\%_{iron\ oxide}$
- Magnetization M in A/m — $M\left[\frac{A}{m}\right] = M\left[\frac{emu}{g}\right] * \rho\left[\frac{g}{cm^3}\right] * 1000$
- Susceptibility χ — $\chi = \frac{M[\frac{A}{m}]}{H[\frac{A}{m}]}, \quad H\left[\frac{A}{m}\right] = H[Oe] * \frac{250}{\pi}$

For the density of iron oxide ($\rho_{iron\ oxide}$) a value of 5350 kg/m³ was used, since this value is given in the data sheet for the pure iron oxide particles. The fraction of iron oxide for the *micromer®-M-NH₂ 10 µm* particles is given as 3 - 6 wt%; for the calculations a mean value of 4.5 wt% was used. The same stands for the *micromer®-M-PEG-COOH 3 µm* particles, for which an iron oxide fraction of 9 - 14 wt% is given and a mean value of 11.5 wt% was used in the calculations. The particle properties given in the data sheets and the calculated values are summarized in Table 3.2.

	Diam. [µm]	Volume [m³]	Iron oxide wt%	Iron oxide V%	Volume iron oxide [m³]	density [kg/m³]	M (H=1000 Oe) [emu/g]	M (H=79577 A/m) [A/m]	χ [1]
iron oxide 250 nm	0.25	$8.181*10^{-21}$	100	100	$8.181*10^{-21}$	5350	46.00	246100	3.09258
micromer®-M-NH₂ 10 µm	10	$5.236*10^{-16}$	4.5	0.93	$4.845*10^{-18}$	1100	1.80	1980	0.02488
micromer®-M-PEG-COOH 3 µm	3	$1.414*10^{-17}$	11.5	2.36	$3.343*10^{-19}$	1100	5.40	5940	0.07464
sicastar®-M 1.5 µm	1.5	$1.767*10^{-18}$	25	11.68	$2.064*10^{-19}$	2500	6.00	15000	0.18850

Table 3.2: Magnetic microparticle properties

3.4 Simulations

To simulate the behavior of the various MPs under the influence of the applied magnetic field gradient due to the different conductor geometries COMSOL Multiphysics version 4.3 was used. The overall power of COMSOL lies in the possibility to couple different physical phenomena while using a comfortable graphical user interface (GUI). To build a model one simply has to define the relevant physical quantities, like material properties, sources and

fluxes instead of defining the underlying equations [20]. Then different type of studies can be performed, such as stationary and time-dependent (transient) studies which are carried out by a corresponding solver. Another useful feature of COMSOL is that the model consists of different nodes forming the model tree, which allows changing a single property of the model while leaving every other aspect as previously selected. Therefore, any part of the model can be easily parameterized. Apart from the built in possibilities several optional add-on modules are available for certain key application areas. For this project the *"AC/DC Module"*, the *"CFD Module"* (computational fluid dynamics) and the *"Particle Tracing Module"* were used.

The model was built in 2D (see Figure 3.13) since a 3D model results in a much bigger computation time and the investigated properties (conductor width, thickness and spacing and the material properties of the MPs) and the current switching times, depending on these properties, can be sufficiently simulated in a 2D model. To simplify the model only 6 conductors were used in the simulation instead of 18 or 10 used in the fabricated chips (see section 4). The conductor properties (width, thickness and spacing), the MP properties (diameter, density and susceptibility) and the current were modeled as parameters so the model can be easily adapted for the different geometries and MPs. The channel has a depth of 15 µm and a length determined by $l = 7 * (c_w + c_s) - 10\ \mu m$, where c_w is the conductor width and c_s the conductor spacing.

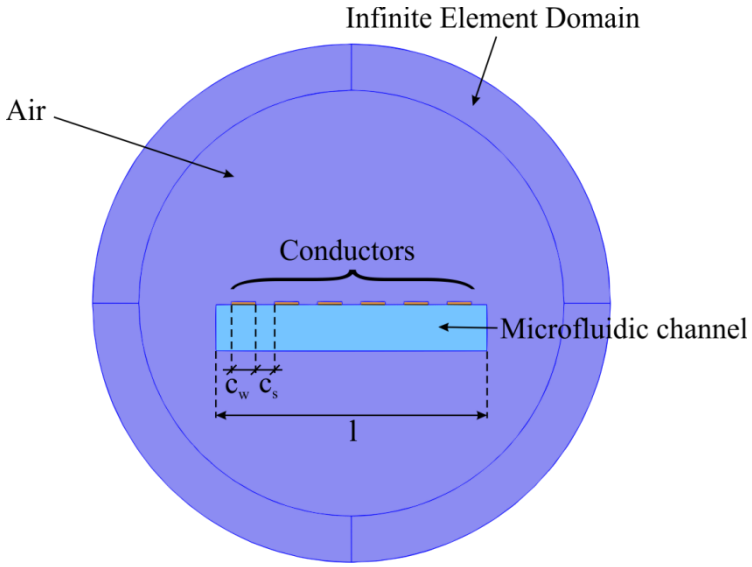

Figure 3.13: COMSOL 2D model, consisting of the microfluidic channel of length *l*, the conductors of width c_w and spacing c_s, surrounding air and the infinite element domain

The geometry of the conductors and the channel is represented by rectangles. The corresponding material is determined using the materials supplied in the COMSOL material browser; copper for the conductors and water for the buffer fluid in the microfluidic channel. Surrounding this geometry is a circle with a radius of half the channel length plus 40 µm and a layer thickness of 15 µm. The circle represents the surrounding air and the layer infinite

element domain (split up into four segments), which is a tool in COMSOL to assure that the solution inside the region of interest is not affected by the presence of artificial boundaries [21]. Therefore a coordinate scaling is applied to the surrounding layer, creating a virtual domain stretched out towards infinity.

The required physics interfaces are selected from the *"Add Physics"* page. From the *"AC/DC"* branch, the *"Magnetic Fields"* interface is used to simulate the magnetic flux density, from the *"Single-Phase Flow"* branch (a sub branch from the *"Fluid Flow"* branch) the *"Creeping Flow"* interface is used to simulate the Stokes flow occurring in microfluidic systems and from the *"Fluid Flow"* branch the *"Particle Tracing for Fluid Flow"* interface is used to simulate the particle movement.

Magnetic Fields Interface

The current running through each conductor is added by *"External Current Density"* nodes in the *"Magnetic Fields"* interface, one node for each conductor. The value for the current density is applied to the z-component of the current density, since this is the out of plane direction in the 2D model and therefore the direction in which the current is flowing.

The currents on the conductors are supposed to be turned on and off sequentially. This means that the first conductor is turned on at the beginning of the simulation and stays on for the duration of a certain interval. When it is turned off the second conductor is turned on for the duration of a certain interval; and so on. To simulate a signal that is turned on during an interval the *"Rectangle"* function can be used. It is "one" during the interval and "zero" else. The interval time of the *"Rectangle"* is defined by the two parameters *"lower limit"* t_{ll} and *"upper limit"* t_{ul}. The *"lower limit"* parameter defines when the function changes its value from "zero" to "one" and *"upper limit"* defines when the function changes its value back to "zero". Figure 3.14 shows an example where t_{ll} = 2 s and t_{ul} = 7 s.

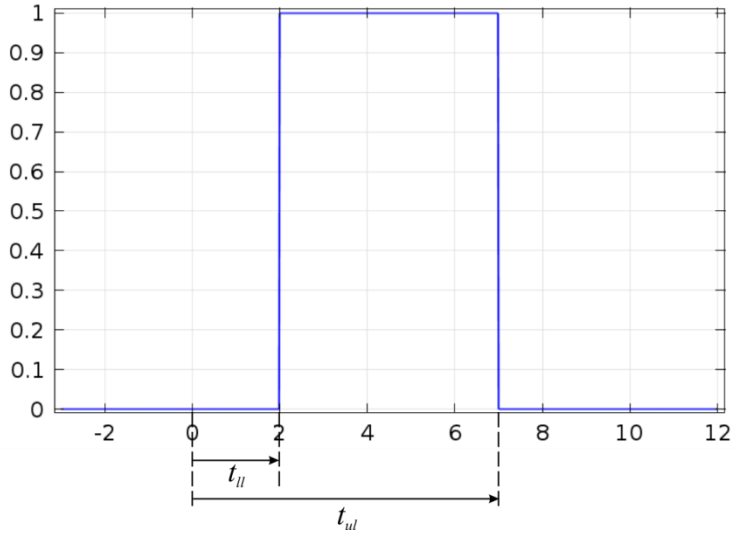

Figure 3.14: *"Rectangle"* function used in COMSOL with time parameters *"lower limit"* t_{ll} (2 s) and *"upper limit"* t_{ul} (7 s)

An important aspect is that the *"Rectangle"* function should not have slopes in form of Heaviside steps, but instead should have transition zones, where these steps are smoothed. Therefore COMSOL provides a "Smoothing" function for the *"Rectangle"* function. This is done to avoid discontinuities which are difficult to handle numerically and produce unwanted behavior in the model [22]. It was found that there has to be at least 5 time steps calculated by a time solver per transition zone to accomplish this, otherwise overshooting of the magnetic flux density could be observed. In Figure 3.15 the *"Smoothing"* is shown. The size of the transition zone is controlled by the time parameter t_s. The *"lower limit"* t_{ll} is set to half the *"Smoothing"* time t_s. Therefore the *"Rectangle"* function begins at the time index "0"; if t_{ll} would be set to "0" the function would start with a negative time index (see Figure 3.15 for an example with t_s = 2 s, t_{ll} = 1 s and t_{ul} = 6 s).

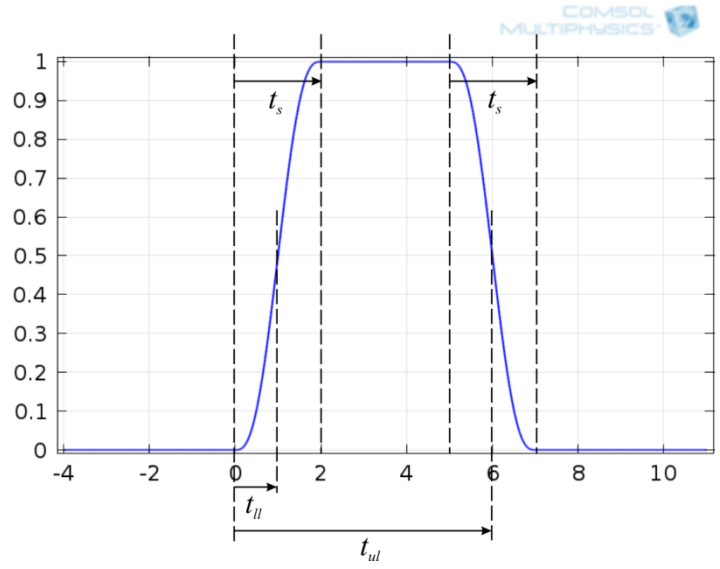

Figure 3.15: Smoothed *"Rectangle"* function used in COMSOL with transition zones of duration t_s (2 s) and time parameters *"lower limit"* t_{ll} (1 s) and *"upper limit"* t_{ul} (6 s)

At the beginning of the simulation the first conductor has to collect the MPs which are being uniformly distributed at the inlet boundary of the channel, corresponding to a uniform distribution of the MPs over the channel depth. Therefore the first conductor has to be turned on for a different duration (MP collection time) than the following ones and for this reason two *"Rectangle"* functions are used in the model. *"Rectangle 1"* is just used for the first conductor and *"Rectangle 2"* for the remaining five conductors. To achieve the required sequence of currents, the *"Rectangle"* functions are multiplied with the magnitude of the current density and time delayed for each *"External Current Density"* node according to the conductor position along the microfluidic channel.

For both *"Rectangle"* functions a corresponding time parameter for the *"upper limit"* is used to control the interval time in which the *"Rectangle"* function is "one". These time parameters are also used for the time delays of the *"Rectangle"* functions and are therefore called t_d and t_{d2}. The parameter t_d is the *"upper limit"* for *"Rectangle 1"* which is used for the first conductor. This parameter is also used as the time delay for the second conductor. The

parameter t_{d2} is the *"upper limit"* for *"Rectangle 2"* which is used for the remaining five conductors. This parameter is also used as the added time delay for conductors three to six. Thus the first conductor has no time delay, the second one a delay of t_d, the third one a delay of $t_d + t_{d2}$, the forth a delay of $t_d + 2*t_{d2}$, and so on (see Figure 3.16). As a consequence of the way the time parameters and the delays were chosen, the *"Rectangle"* functions for the conductors overlap for a small time duration. Hence the current density for the next conductor starts to rise while the current density for the previous conductor is not set "zero" (see Figure 3.16). The parameters where chosen this way to achieve a more fluent movement of the MPs.

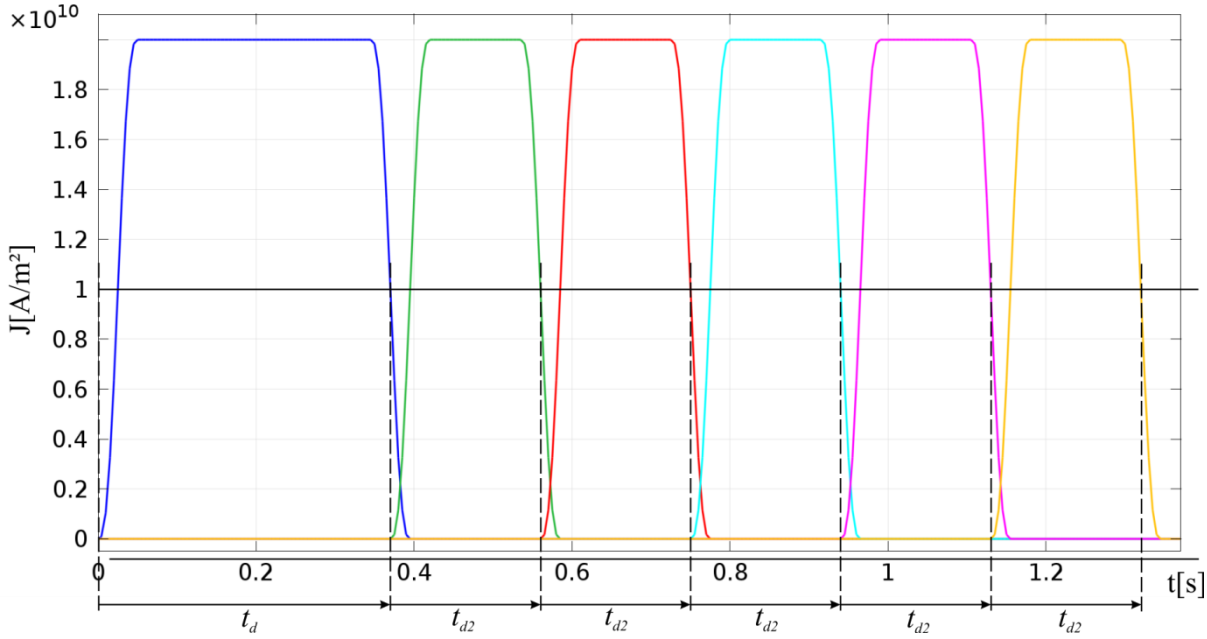

Figure 3.16: Current density plot (COMSOL) for the six conductors of the model (each conductor in a different color) with time delay parameters t_d = 0.37 and t_{d2} = 0.19. (Plotted for the SI-geometry and the *micromer®-M-NH₂ 10 µm* particles)

Creeping Flow Interface

As described above the *"Creeping Flow"* Interface is used to simulate the Stokes flow occurring in microfluidic systems. The *"Fluid Properties"* and also the inlet and outlet of the microfluidic channel are defined through according *"Inlet"* and *"Outlet"* nodes. Another use of this interface is to be able to establish an inflow velocity at the inlet if it is decided that an external fluid flow is applied to the channel later on in the project.

Particle Tracing for Fluid Flow Interface

This interface computes the motion of particles in a fluid. In the *"Particle Properties"* node the particle density and diameter are defined; in the *"Wall"* node the "*Wall Condition*" for the microfluidic channel is set to *"Bounce"*, so that particles are reflected from the channel boundaries and keep their momentum; *"Inlet"* and *"Outlet"* are defined in their respective

nodes, with the *"Inlet"* releasing 100 particles uniformly distributed over the boundary of the inlet at the beginning of simulation and finally nodes are added for the drag force and the magnetophoretic force. In the *"Drag Force"* node the velocity field is defined as the one calculated from the *"Creeping Flow"* interface. In the *"Magnetophoretic"* node the magnetic field calculated in the *"Magnetic Fields"* interface is selected for the occurring field and the relative permeability of the particle $\mu_{r,p}$ and the fluid $\mu_{r,f}$ are defined, $\mu_{r,f}$ being 1 and $\mu_{r,p} = 1 + \chi_p$, where χ_p is the particle susceptibility.

Mesh

Since COMSOL uses the finite-element method to solve models, the continuous domains of the model have to be discretized by a number of discrete sub-domains called finite-elements. This is done by building a mesh. The conductor, microfluidic channel and the infinite element domains are meshed using *"Mapped"* nodes which create structured quadrilateral meshes. The number, size and distribution of elements are controlled by *"Distribution"* subnodes. Since the microfluidic channel is the region of interest in the model, the mesh is designed to be rather dense, using *"Distribution"* subnodes for the horizontal and vertical boundary of the channel. The remaining domain, representing the surrounding air is meshed by a *"Free Triangular"* node, which creates an unstructured triangular mesh. Here the number, size and distribution of elements are controlled by a *"Size"* subnode, and since this region is not important for the model, the predefined coarse value was used. The resulting mesh can be seen in Figure 3.17.

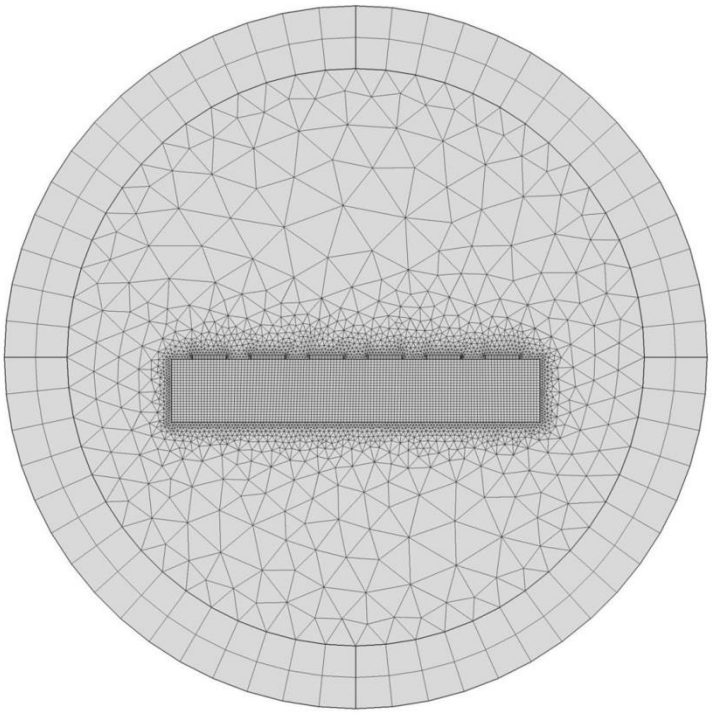

Figure 3.17: Mesh for the 2D model in COMSOL

Additional considerations

The different MPs react to the magnetic field according to their magnetic volume (volume of iron oxide in Table 3.2). This means that MPs with bigger magnetic volume will react stronger and therefore move faster. In consequence the time delay parameters t_d and t_{d2} for the *"Rectangle"* functions will have to get smaller. As shown in Figure 3.15 the time parameter t_s is used for both transition zones of the *"Rectangle"* function. Therefore t_s must always be smaller than half the width of the *"Rectangle"* function; otherwise the function would not reach the value "one". Hence the rectangle interval times and therefore the time delay parameters cannot get below a certain value for a given transition time t_s. Therefore if the interval time has to be reduced, the transition time has to be also shortened. As a consequence the time steps of the solver also have to be smaller, because the transition zones have to be resolved by at least five time steps to avoid unwanted behavior in the model as pointed out earlier. An easy solution would be to use small transition zones with the according time steps for all simulations, but because the computation time is directly related to the amount of time steps calculated, this solution was not chosen. Instead optimal values were found iteratively for each MP, meaning that the time steps and transition times were always the same for each individual MP when simulated with the different conductor geometries and were therefore comparable with each other. The values found for the time steps and the transition times can be seen in Table 3.3.

	Time steps [s]	Transition time [s]
iron oxide 250 nm	0.05	0.4
sicastar®-M 1.5 µm	0.04	0.2
micromer®-M-PEG-COOH 3 µm	0.02	0.1
micromer®-M-NH_2 10 µm	0.01	0.05

Table 3.3: Simulation time steps and *"Rectangle"* transition times used for the different MPs

The goal of the simulations was to find the optimal conductor geometry, and therefore the geometry which transports the MPs as fast as possible. The time the MPs need to travel through the microfluidic channel depends on the magnitude of attraction to the conductors, therefore on the current, which in turn depends on the conductor cross section. Additionally the time depends on the distance the MPs have to travel. Because of that not all geometries listed in Table 3.1 were simulated, but only one for each conductor width, namely the one with the smaller conductor spacing, hence the shorter distance for the particles to travel. The five simulated geometries were the GE I (12/8 µm), G I (10/8 µm), S III (8/6 µm), S I (6/5 µm) and S (4/4 µm); the values in brackets stand for the conductor width/spacing.

Simulations

The simulations were carried out for a conductor thickness of 1 µm and the current values given in Table 3.1. A simulation for every combination of the five chosen geometries and the five particles listed in Table 3.2 was carried out. For each simulation the smallest possible values of the time delay parameters t_d and t_{d2} were found by iteratively adapting them until an optimum solution was achieved, consisting of the shortest times while still managing to transport the MPs through the channel. Table 3.4 shows the resulting values for the time delay parameters for all 20 simulations.

	GE I (12/8 µm)		G I (10/8 µm)		S III (8/6 µm)		S I (6/5 µm)		S (4/4 µm)	
	t_d	t_{d2}	t_d	t_{d2}	t_d	t_{d2}	t_d	t_{d2}	t_d	t_{d2}
	[s]		[s]		[s]		[s]		[s]	
iron oxide 250 nm	6	10.3	6.9	9.3	6.7	5.5	8.6	3.7	15.1	2.2
sicastar®-M 1.5 µm	1.52	2.68	1.68	2.44	1.68	1.52	2.16	1.16	3.72	0.68
micromer®-M-PEG-COOH 3 µm	0.92	1.62	1.02	1.48	1.02	0.88	1.3	0.66	2.26	0.42
micromer®-M-NH_2 10 µm	0.27	0.49	0.3	0.42	0.29	0.29	0.37	0.19	0.63	0.13

Table 3.4: Time delay parameters t_d and t_{d2} in s for the different conductor geometries and MPs

Particle velocity calculations

The times the particles required to reach the last conductor were noted and the mean velocities achieved by the MPs were calculated by dividing the traveled distance through these times. This was performed for two starting points of the MPs, the first being the inlet of the microfluidic channel and the second the edge of the first conductor facing the channel inlet. The 1st scenario includes the already mentioned collection of the MPs which is done by the first conductor. The 2nd scenario discards this influence. In Figure 3.18 a particle tracing plot of COMSOL is shown including the discussed starting points, the end point and the respective travel distances for the particle velocity calculations. Charts of the mean particle velocities are shown in Figure 3.19 for the 1st scenario and in Figure 3.20 for the 2nd scenario.

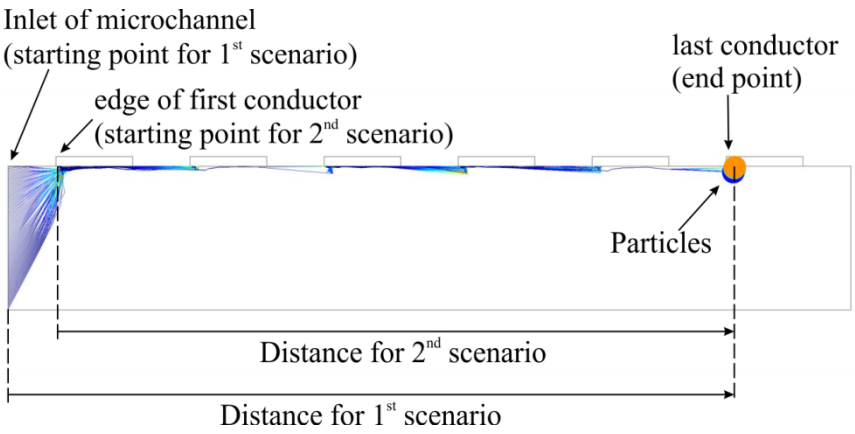

Figure 3.18: Particle tracing plot (COMSOL) with starting points, end point and the distances the particles travel for the two scenarios of the particle velocity calculation

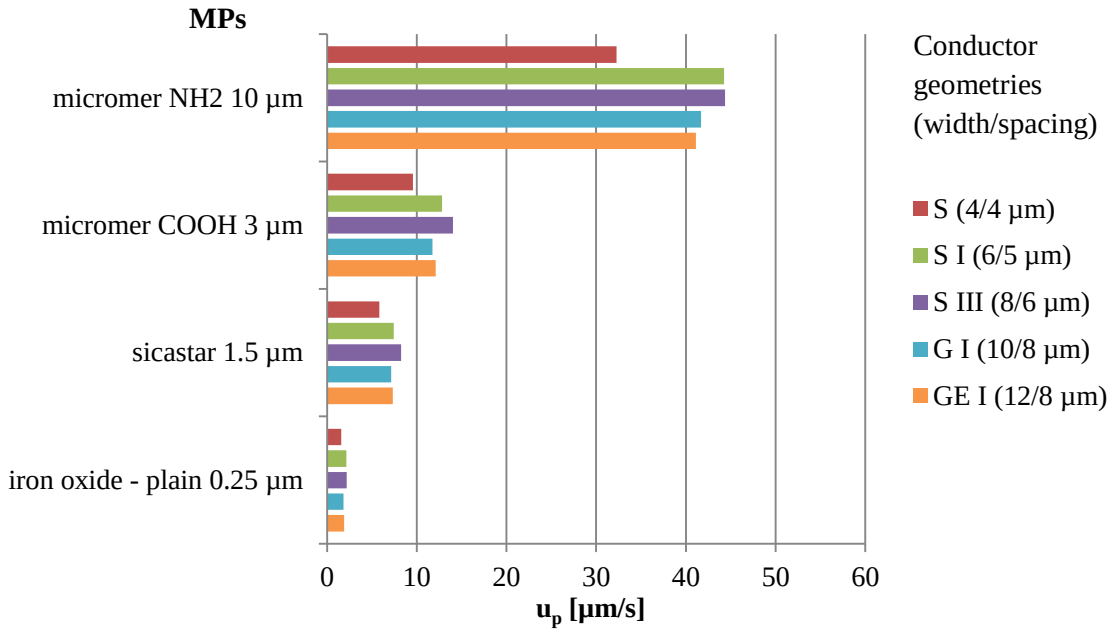

Figure 3.19: Mean particle velocities u_p for different conductor geometries and different MPs, 1st scenario with the inlet of the microchannel as the starting point

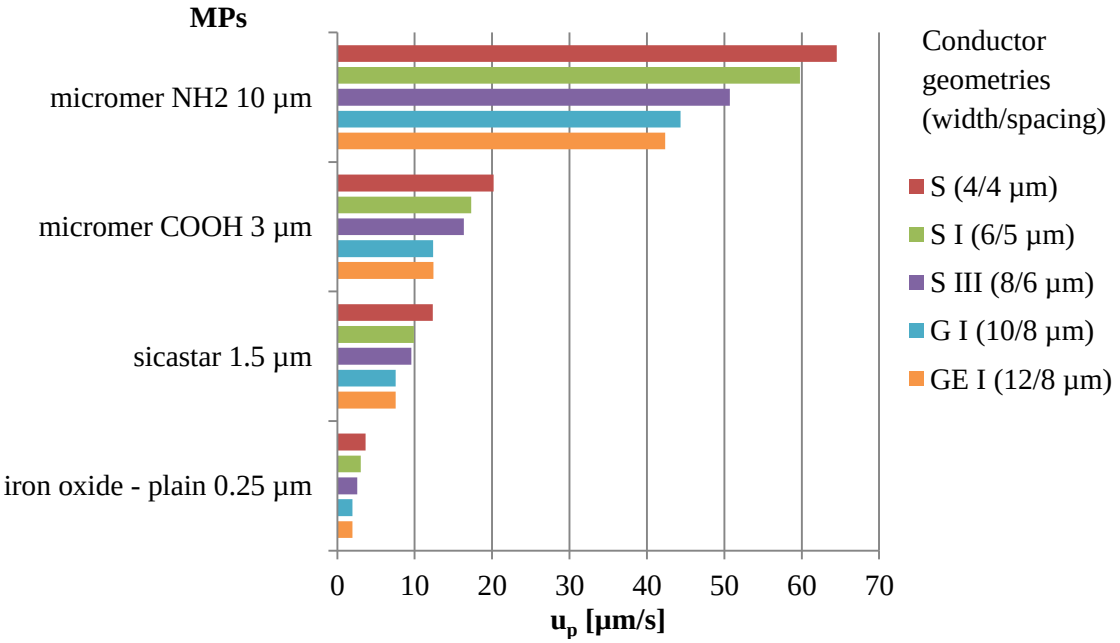

Figure 3.20: Mean particle velocities u_p for different conductor geometries and different MPs, 2nd scenario with the first conductor as the starting point

The response concerning the different MPs is according to the magnetic volume listed in Table 3.2, the *micromer®-M-NH2 10 µm* being the particles with the biggest magnetic

volume and therefore the fastest, and the *iron oxide 250 nm* particles having the smallest magnetic volume and therefore being the slowest.

The 2nd scenario (Figure 3.20), which discards the influence of the MP collection time, shows that the smaller conductor geometries result in a faster particle movement than the bigger ones. This occurs although the currents are lower in the smaller conductors and therefore also the magnetic force is lower. Because of the shorter distances that the particles have to travel, the smaller conductor geometries still produce higher velocities. The higher currents of the bigger conductors come into play when the collecting of MPs is taken into consideration (1st scenario). Here the smallest conductor geometries produce lower mean velocities than the bigger conductor geometries (see Figure 3.19). Considering the simulations were only done for six conductors this influence is higher than in reality.

Figure 3.21 shows an estimation based on the time delay parameters for geometries consisting of 18 conductors; here the particle collecting influence is almost eliminated. In conclusion this means that the smallest producible conductor geometries should be preferred.

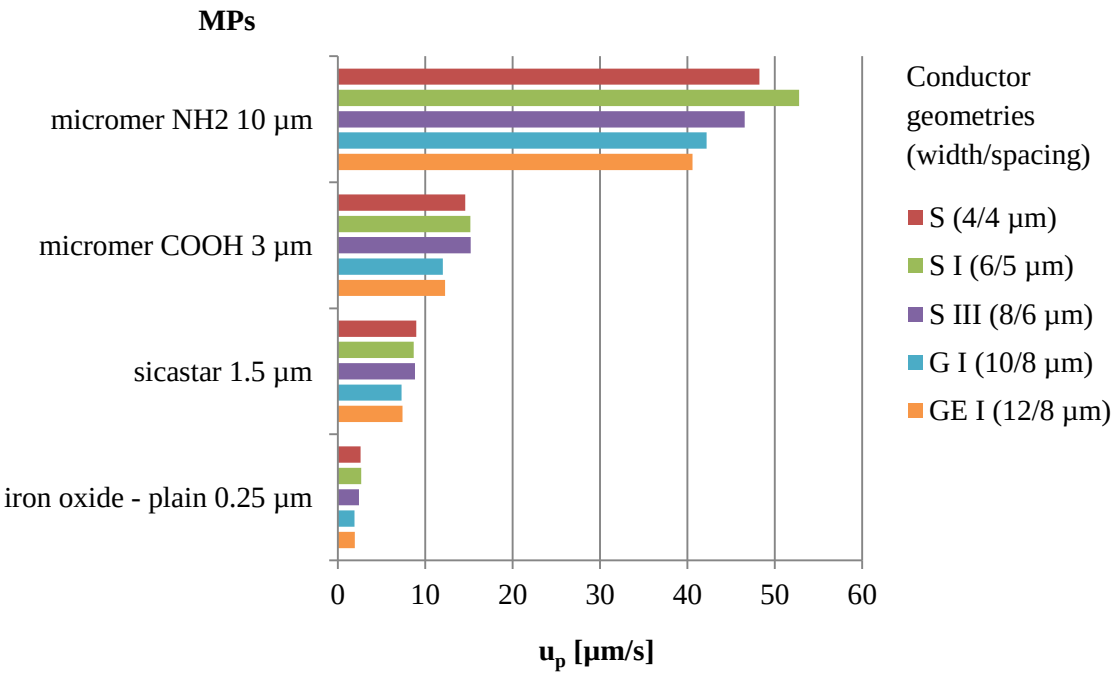

Figure 3.21: Estimated mean particle velocities u_p for different conductor geometries with 18 conductors and different MPs, starting point: beginning of microchannel

4 Chip Development and Characterization

In order to verify the working principle described in section 3.1 a microfluidic chip was developed. The next sections describe the design (section 4.1) and the fabrication of the chip (section 4.2) as well as the experimental set-up (section 4.3) and the measurements that where conducted (section 4.4).

4.1 Chip design

The principle design of the biosensing system previously described in section 3.3, consists of a microfluidic channel with one inlet and one outlet, placed on top of a layer with current carrying microstructures to establish the needed magnetic field gradient. The developed chips consisted of four main layers: (1) A Si-wafer with 500 µm thickness as the substrate, (2) the current carrying conductors which consist of silver with 500 nm thickness and an insulating layer of SiO_2 with 500 nm thickness, (3) the microfluidic channel, structured by two layers of a dry photoresist thin film (Ordyl SY355) of 55 µm thickness giving a total thickness of 110 µm and (4) a glass cover with 500 µm thickness with holes to access the inlets and outlets.

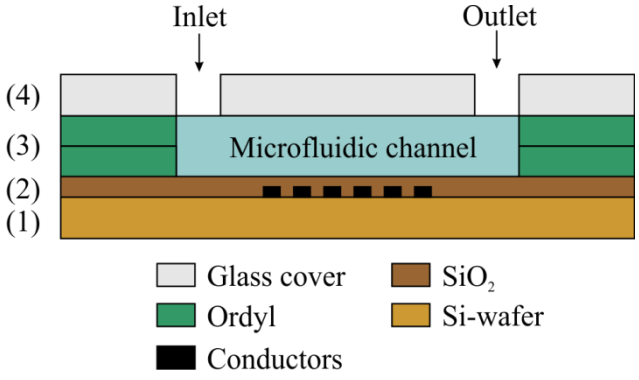

Figure 4.1: Chip layers: (1) Si-wafer as the substrate, (2) the current carrying microstructures and an insulating layer of SiO_2, (3) microfluidic channel made of two layers of Ordyl SY355, (4) glass cover

The microstructures consisted of parallel straight rectangular conductors, with a common contact pad on one end of the conductors and individual pads on the other end. Hence, it is

possible to individually actuate the conductors. Chips with geometries (conductor width and spacing) G I, G II, G III, and GE I (see Table 3.1) consisting of 18 conductors were produced, as well as chips with 10 conductors with geometry G I. The microfluidic channel layer consisted of two individual channels with a width of 100 µm and one inlet and outlet each. The channels were oriented perpendicular to the conductors. Figure 4.2 shows a schematic of the conductor layer for geometry G I with 18 conductors with their conductor pads and of the microfluidic layer consisting of the two channels with their inlets and outlets.

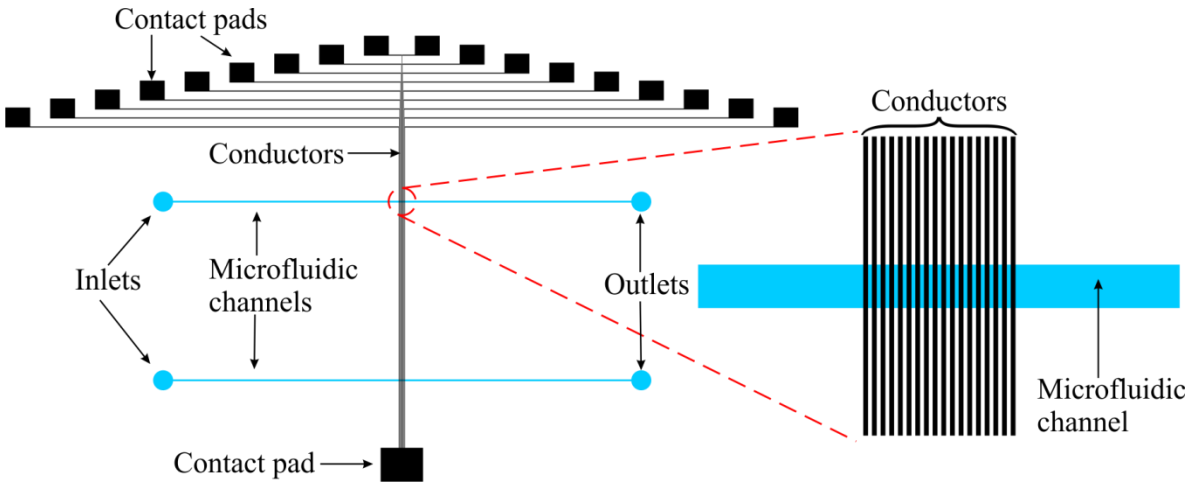

Figure 4.2: Schematic of the current carrying microstructure (conductors and contact pads, G I geometry) and microfluidic channels with inlets and outlets, as used for the masks for fabrication

4.2 Fabrication

4.2.1 Conductors

The conductors were fabricated in the clean room of the institute using standard fabrication procedures. A Si-wafer (10 cm diameter, 500 µm thickness) with a thermally grown oxide was used as the bottom substrate. Figure 4.3 depicts the fabrication steps.

a) An image reversal photoresist (AZ5214) was spin coated on the Si-wafer
b) The photoresist was exposed using a mask for the patterning of the microstructures
c) The photoresist was developed
d) 500 nm of silver with a 30 nm adhesion layer of titanium was evaporated on the Si wafer
e) After the silver was deposited, the photoresist was stripped using acetone and the remaining debris of the resist was cleaned using oxygen plasma

f) An insulating layer of SiO_2 with 500 nm thickness was plasma deposited on top of the conductors
g) Photoresist was spin coated on top of the SiO_2 layer
h) The photoresist was exposed using a mask for openings in the SiO_2 layer to free the contact pads
i) The photoresist was developed
j) Plasma etching was employed to free the contact pads
k) The photoresist was stripped

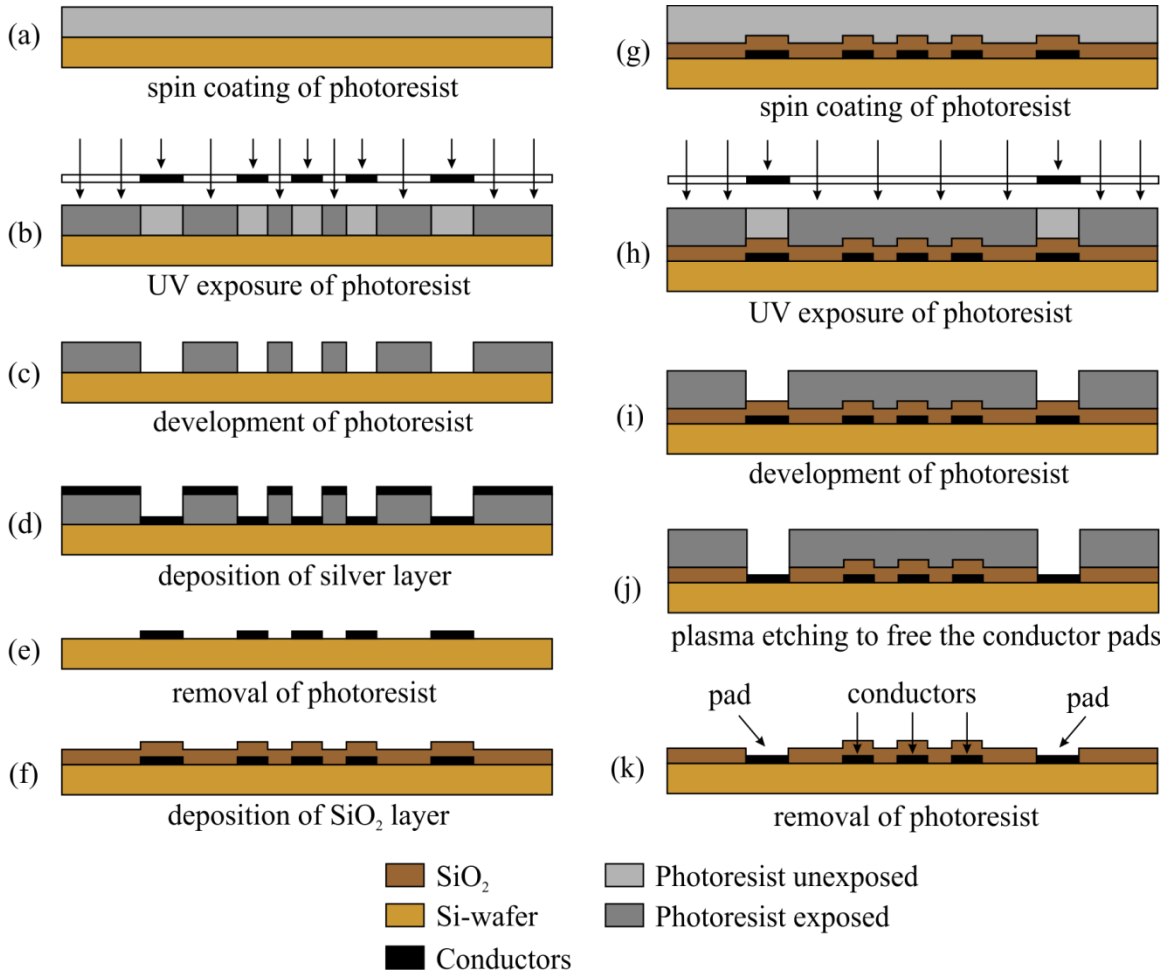

Figure 4.3: Conductor fabrication steps

4.2.2 Microfluidic channel

The microfluidic channel layer was made of Ordyl SY300, a negative-type dry-film photoresist, manufactured by Elga Europe. It is available in thicknesses from 15 µm to 55µm; for the microfluidic channel two layers of 55 µm (Ordyl SY355) were utilized.

There are several reasons why a dry-film photoresist was used:

- Easy to handle
- Low cost
- Ordyl can be used for direct adhesive bonding under pressure and elevated temperature
- Other materials for adhesive bonding like SU-8 photoresist have to be applied by spin coating, which is an inhomogeneous deposition and therefore limits the maximum resist thickness

The photoresist film is encapsulated in two protective layers. A polyester (PET) layer on one side and a polyethylene (PE) layer on the other side. The exact composition and functioning of Ordyl is a trade secret, but it is known that it contains roughly 60% acrylic polymers and 25% acrylic esters [23]. The acrylic esters contain epoxy groups that establish bonds to the substrate surface after cross-linking is photochemically initiated (by UV exposure) and promoted with a post-exposure bake (PEB). During the bonding step the epoxy groups also form bonds to a second substrate surface. Thus it is possible to directly bond one substrate with an Ordyl layer to a second bare substrate without the need of an intermediate adhesive layer. [23]

Processing Ordyl consists of four major steps (see Figure 4.4):

a) Lamination of the dry film to the bottom substrate
b) UV exposure with a mask to pattern the desired structure
c) Development
d) Direct adhesive bonding to top and bottom substrate under pressure and elevated temperature

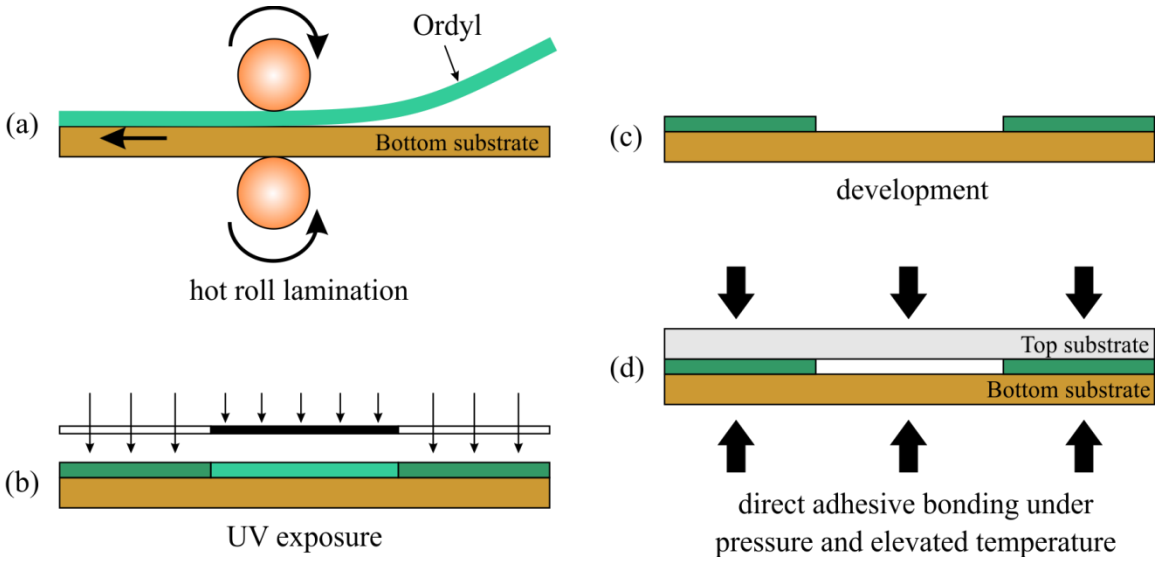

Figure 4.4: Ordyl processing steps

Lamination

A GBC HeatSeal H425 standard office laminator was used to laminate the Ordyl SY355 film onto the bottom substrate (the previously processed Si-wafer with the patterned silver conductor microstructures on top). The wafer was put on a piece of paper and a sheet of Ordyl was cut out in a way that it covers the wafer completely, but does not exceed the borders of the paper, thus preventing that it gets in contact with the laminator rolls. The top of the Ordyl film was attached to the paper with a piece of adhesive tape, the side with the protective PE layer facing the wafer. The protective PE layer was removed and the whole stack was inserted into the laminator. To prevent bubbles or folding, the dry film must not be in contact with the wafer prior lamination. To assure this the photoresist was continuously lifted during lamination as depictured in Figure 4.5 [24]. The lamination speed was 400 mm per minute, the temperature is not specified in the laminator manual, but a setting of “6” from a range from “1” to “9” was proven to be appropriate. After lamination the overlaying parts of the Ordyl sheet were cut away with a knife. Because a second layer of Ordyl was needed, the protective PET layer was removed from the already laminated layer and the entire process was repeated with another sheet of Ordyl. The PET layer of the second resist sheet was kept on top to prevent the Ordyl surface from oxidation and to prevent mechanical contact with the mask in the mask aligner during UV-exposure.

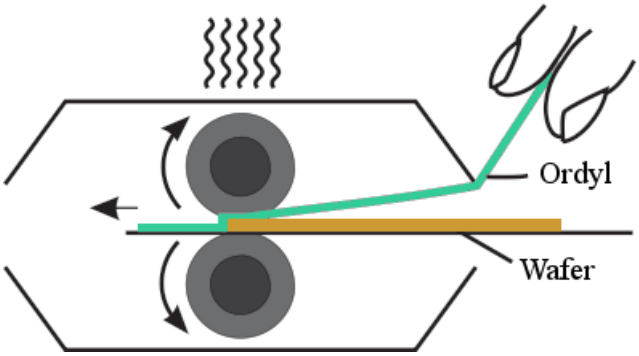

Figure 4.5: To prevent bubbles or folding the Ordyl sheet is lifted during lamination, so that it does not touch the wafer before lamination. [24]

Exposure and development

A Süss MA6 mask aligner was used to expose the photoresist for 45 s using soft-contact mode with the protective PET layer still on top during exposure. After exposure the PET layer was removed and the wafer was post-exposure baked by putting it on a hot plate at 85 °C for 60 s. Afterwards the resist was developed in a commercial developer (Elga Europe) utilizing two developer baths, first an already used one (2 min) followed by a clean developer bath (2 min). Ultrasonic actuation was used to reduce development times. The waver was cleaned in an isopropanol bath (30 s) and rinsed with DI-water.

4.2.3 Glass-cover

Hole drilling

To cover the microfluidic channels a glass-wafer was utilized as the top layer of the chip. To enable access to the microfluidic channels, holes had to be drilled in the glass-wafer before bonding with the Ordyl layer. 800 µm holes were drilled with a diamond drill to form the inlets and outlets.

Wafer bonding

The Si-wafer and the glass-wafer were aligned, secured with a bond tool and inserted into an EVG 501 wafer bonder. The wafers were bonded by applying a force of 60 N / cm². The temperature was increased to 100 °C with 5 °C / min and maintained for 30 minutes. Afterwards the temperature was reduced to room temperature at 1 °C / min.

4.2.4 Dicing

To cut the bonded wafers into single chips a DAD 3220 dicing saw with a 200 µm thick diamond blade was used. The inlet and outlet holes in the glass-wafer were sealed with adhesive tape before dicing to prevent cooling water and debris from entering the chips. To free the contact pads, the glass wafer was partially removed in the areas above the pads. This was done by dicing the chip half through; dicing only through the glass-wafer and using the Ordyl layer as spacer that prevented the conductors and contact pads from getting damaged.

4.3 Experimental Set-up

To actuate the currents on the conductors an Arduino Uno [25] microcontroller board was used. It is an open-source electronics prototyping platform based on the ATmega328 microcontroller. It incorporates, among other features, 14 digital input/output pins and is easy to program with the Arduino programming software. An HP Notebook connected to the Arduino via USB was used for programming. 8 of the digital input/output pins were programmed as outputs to actuate the conductors on the microfluidic chip. A program was written that sequentially turns the outputs on for a specified duration (actuation time). The outputs of the microcontroller board were connected to a solderless breadboard where MOSFETs act as switches between the conductors of the microfluidic chip and an external DC power supply. LEDs were used to visualize when a conductor was turned on. Additional

to the ability of the power supply to limit the outgoing current, an amperemeter was used to monitor the current running through the conductors.

To contact the conductor pads on the microfluidic chip, copper wire was used. In a first attempt a silver conductive paint was used for connection, but since the paint did not provide a strong enough adhesion to the pads, conductive silver epoxy was used. To connect the chip to the microcontroller circuit a custom made connector was produced. It consists of an 8 way PCB vertical mount terminal, connected to a 15 way IDC plastic body D-sub plug with a flat ribbon cable. Another flat ribbon cable with a D-sub socket and a D-sub plug was used to make the connection to the bread board. To enable heat transport away from the chip it was placed on a copper block and fixed with adhesive tape.

A Carl Zeiss microscope with an attached Samsung VP-HMX20C camcorder was used to capture the movement of the MPs in the microfluidic channel. In Figure 4.6 the entire measurement set-up is shown.

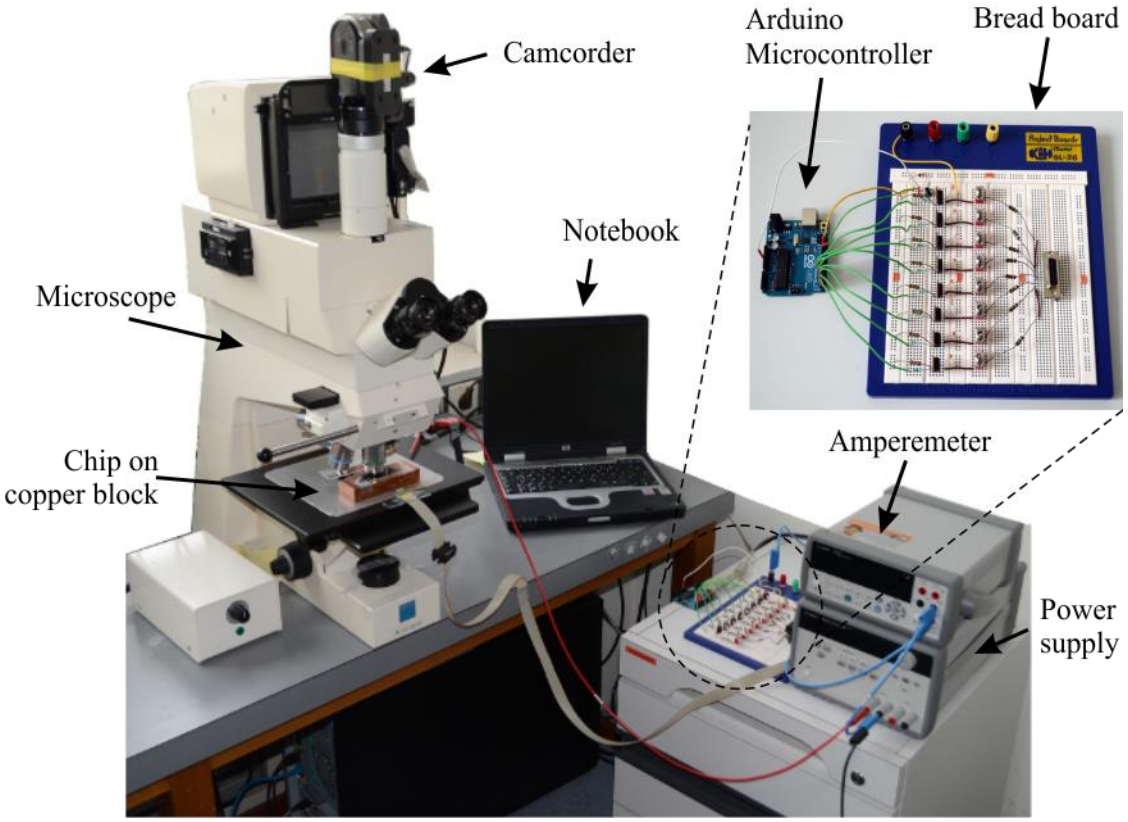

Figure 4.6: Measurement set-up

4.4 Measurements

For all measurements the particle solutions were resuspended in Hellmanex® cleaning concentrate (dilution of 1:50 with DI-water). According to [12] the high pH (11) and the surfactant in Hellmanex® increase the repulsive electrical forces between particles and solid surface, thus avoiding particle clustering or adhesion of the particles on the solid surface.

The particles purchased from micromod Partikeltechnologie GmbH come in tubes with 10 mL content (particles suspended in water). Figure 4.7 shows a photograph of three tubes with magnetic particles (brown) and one with white non-magnetic particles. The white particles were used to form LMPs (see section 4.4.2).

Figure 4.7: Magnetic particles (three tubes on top with brown content) and non-magnetic particles (tube on bottom with white content) purchased from micromod Partikeltechnologie GmbH

To administer the particle solutions to the microfluidic channel a 1 mL syringe, a 0.8 mm cannula and a piece of rubber tube were combined (see Figure 4.8).

Figure 4.8: A 1 mL syringe, a 0.8 mm cannula and a piece of rubber tube (top) that were combined (bottom) to create a tool for administering the particle solutions to the microfluidic channel

For each experiment a small amount of particle solution was drawn into the syringe, the rubber tube end was placed on the inlet of the microfluidic channel and the particle solution was brought into the channel by carefully administering pressure on the syringe. The same tool was used to clean the channel after each experiment by flushing it with DI-water and ethanol; for each fluid different syringes and cannulas were used.

First tests utilizing a chip with G II geometry (c_w = 10 µm, c_s = 10 µm) showed that applying a current of 100 mA (the maximum value for this conductor width according to Table 3.1) caused the conductors getting destroyed after just some actuations. Therefore all following experiments were done with half the current value listed in Table 3.1.

4.4.1 MPs

Experiments with different bare MPs were carried out to verify the behavior suggested by the simulations presented in section 3.4. The conductors on a chip with G I geometry (c_w = 10 µm, c_s = 8 µm) were actuated with a current of I = 50 mA. To determine the maximum mean particle velocities (u_p) that were feasible with this configuration two approaches were followed:

- For the *micromer®-M-NH$_2$ 10 µm* and *micromer®-M-PEG-COOH 3 µm* particles the minimum actuation time (during which the current is switched on, on each conductor) was determined by lowering the actuation time in the Arduino program until the transport of MPs through the channel was no longer guaranteed.

- Since the smaller *sicastar®-M 1.5 µm* and *iron oxide 250 nm* particles travel slower in the channel, the process of finding the right actuation time was accelerated by switching the conductors manually on and extracting the actuation time from the video footage by determining the time it took the MPs to travel from one conductor to the next one.

Table 4.1 lists the actuation times and the corresponding mean particle velocities. The determined mean velocities correspond to the velocities calculated via the simulations in section 3.4, meaning that the four measured MPs show the same ranking as in the simulations: the 10 µm MP being the fastest and the 250 nm MP being the slowest. Figure 4.9 depicts the movement of a *micromer®-M-NH$_2$ 10 µm* MP along the microfluidic channel with the determined actuation time of 1.2 s. The position of the MP is pictured every 0.6 s travelling a distance of 108 µm with a mean velocity of 15 µm / s.

Particle	Actuation time [s]	u_p [µm / s]
micromer®-M-NH$_2$ 10 µm	1.2	15
micromer®-M-PEG-COOH 3 µm	2.3	7.8
sicastar®-M 1.5 µm	3.8	4.7
iron oxide 250 nm	11.5	1.6

Table 4.1: Actuation times and mean particle velocities u_p for different MPs travelling in a G I geometry (c_w = 10 µm, c_s = 8 µm) chip, actuated with a current of I = 50 mA

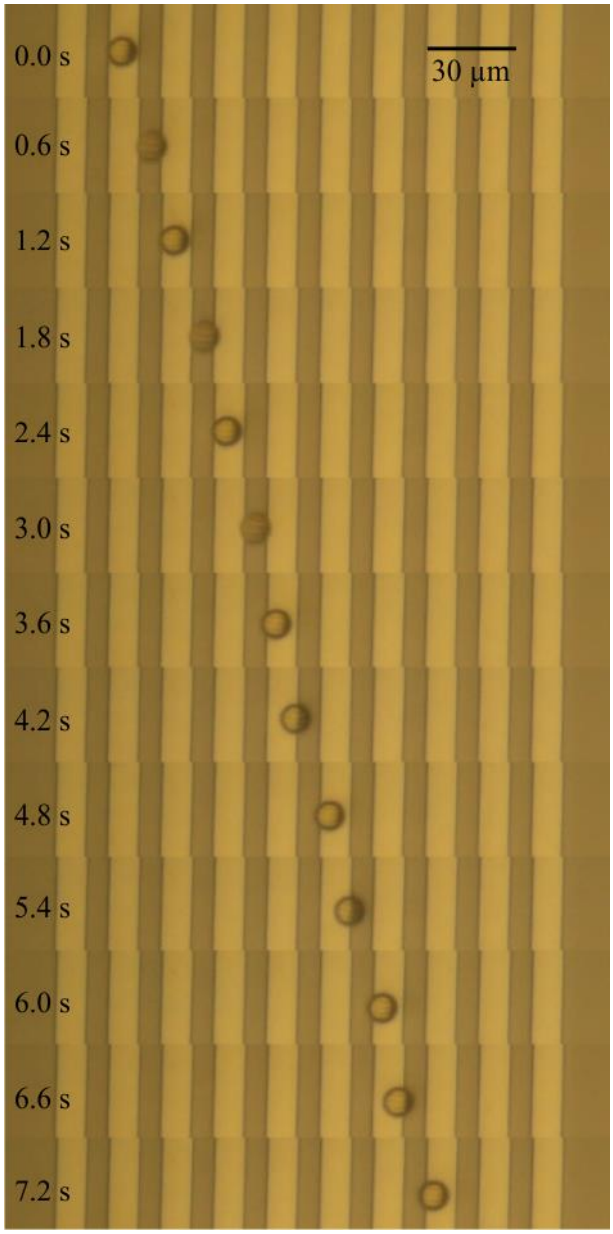

Figure 4.9: Movement of a *micromer®-M-NH$_2$ 10 µm* MP along the microfluidic channel with an actuation time of 1.2 s per conductor (G I geometry: c_w = 10 µm, c_s = 8 µm). The current was I = 50 mA. The MP covered a distance of 108 µm with a mean velocity of 15 µm / s

4.4.2 LMPs

To form LMPs the protocol given in [26] was taken as a reference. It utilizes the carbodiimide / N-hydroxysuccinimide activation of the carboxylic acid groups on functionalized particle surfaces, followed by reaction with amino groups of biomolecules to form amid bonds. Instead of bioanalyte, non-magnetic white microparticles with a functionalized amino group surfaced were used as a proof of concept. Specifically *micromer®-M-PEG-COOH 3 µm* with carboxylic acid groups on their surface where used as MPs, and to simulate the bioanalyte, *micromer®-NH_2 500 nm* white non-magnetic particles with amino groups on their surface were used.

As stated in the protocol [26] a 0.5 M MES buffer (2-(4-morpholino)ethanesulphonic acid buffer) solution with an adjusted (more basic) pH had to be prepared. MES has a molecular weight of 195.2 g / mol, this means for a 0.5 M solution 97.6 g / L are required. To have a sufficient amount for future experiments 40 mL of buffer solution was prepared. This was done by first diluting 3.904 g MES (the amount required for a 40 mL solution of 0.5 M MES) in 30 mL DI-water in a 50 mL reaction tube. The measured pH was 3.9. Then 1 g of Na_2CO_3 (sodium carbonite) was diluted in the solution and the reaction tube was filled to the 40 mL mark with DI-water. The measured pH was 6.8.

To quench the reaction a solution of 25 mM glycine in 0.01 M PBS buffer was also prepared. Glycine has a molecular weight of 75.07 g / mol. For a 25 mM solution 1.88 g / L are required. Again, to have a sufficient amount for future experiments 10 mL of solution was prepared. This was done by adding 18.8 mg of glycine to a 10 mL reaction tube and filling it up with 0.01 M PBS buffer to the 10 mL mark.

Following the protocol [26], in a first step, 625 µL of activated *micromer®-M-PEG-COOH 3 µm* particle suspension were produced:

- 0.5 mL of *micromer®-M-PEG-COOH 3 µm* particle suspension (25 mg of particles) were transferred into a 1.75 mL reaction tube
- 4 mg of EDC (1-ethyl-3-(3-dimethylaminopropyl)-carbodiimide hydrochloride) and 8 mg of NHS (N-hydroxysuccinimide), were dissolved in 125 µL of 0.5 M MES (pH 6.8) and added to the particle suspension
- The particle suspension was incubated with continuous shaking for 45 min at room temperature
- The particles were washed 3 times by magnetic separation with 0.01 M PBS buffer
- The particles were resuspended in 625 µL 0.01 M PBS buffer solution

Then 5 batches were prepared. 0.5 mL of *micromer®-NH2 500 nm* white non-magnetic particle suspensions (25 mg of particles) were added to each of 5 1.75 mL reaction tubes. Table 4.2 (batches 1 to 5) lists the amount of activated *micromer®-M-PEG-COOH 3 µm* particle suspension and PBS buffer that was added to each reaction tube.

The steps that followed were the following:

- The suspensions were incubated with continuous mixing overnight at room temperature
- The particles were washed 3 times by magnetic separation with 0.01 M PBS buffer
- 200 µL of 25 mM glycine in 0.01 M PBS buffer was added to each batch to quench the reaction
- The suspensions were incubated with continuous mixing for 30 min at room temperature
- The particles were washed 3 times by magnetic separation with 0.01 M PBS buffer
- The particles were resuspended in 1 mL 0.01 M PBS buffer solution

Additionally in a second run another five batches were made with lesser concentration of activated particle suspensions, see Table 4.2 batches "a" to "e".

Batch	activated magnetic particle suspension [µL]	PBS [µL]
1	25	975
2	75	925
3	125	875
4	175	825
5	225	775
a	5	995
b	10	990
c	15	985
d	20	980
e	25	975

Table 4.2: Amount of activated magnetic particle suspension (*micromer®-M-PEG-COOH 3 µm*) and PBS used for forming of LMPs

The various batches with different concentration of activated particle suspension were made because the protocol given in [26] is intended for the formation of amid bonds between functionalized particles and proteins or antibodies. It was found that the particle-particle bonding worked quite well for all these concentrations but in the higher concentrated suspensions (batch 2 to 5) the tendency that particle clusters formed seemed to be higher.

For the experiment batch "c" was used. Like the bare MPs, the LMPs were resuspended in Hellmanex® (dilution of 1:50 with DI-water). To have a direct comparison to the bare *micromer®-M-PEG-COOH 3 µm* MPs the same chip and current was used as for the measurements described in section 4.4.1. At first the actuation time was set to 2.3 s; the value which was found for the bare 3 µm MP (see Table 3.1). With this value it was not possible to transport the LMP through the channel. This already proofed that the LMP was bigger than

the MP. Then the actuation time was increased until the LMP could be transported through the channel. Table 4.3 shows a comparison between the actuation times and the corresponding mean particle velocities of the bare *micromer®-M-PEG-COOH 3 µm* MP and the LMP with attached 500 nm non-magnetic particles.

Particle	Actuation time [s]	u_p [µm / s]
3 µm MP	2.3	7.8
3 µm + 500 nm LMP	3	6

Table 4.3: Comparison between the actuation times and the corresponding mean particle velocities u_p of the bare *micromer®-M-PEG-COOH 3 µm* MP and the LMP with attached 500 nm non-magnetic particles travelling in a G I geometry (c_w = 10 µm, c_s = 8 µm) chip, actuated with a current of I = 50 mA

The experiment showed a velocity reduction of about 23 % for the LMP against the bare MP. This corresponds well to a theoretical velocity reduction of 25 % for an LMP consisting of a 3 µm MP plus attached 500 nm analyte compared to a bare 3 µm MP (see section 3.2.1 and Figure 3.2). Figure 4.10 shows a comparison of the experiments of the bare *micromer®-M-PEG-COOH 3 µm* MP and the LMP with attached 500 nm non-magnetic particles along the microfluidic channel with the determined actuation times of 2.3 s (MP) and 3 s (LMP).

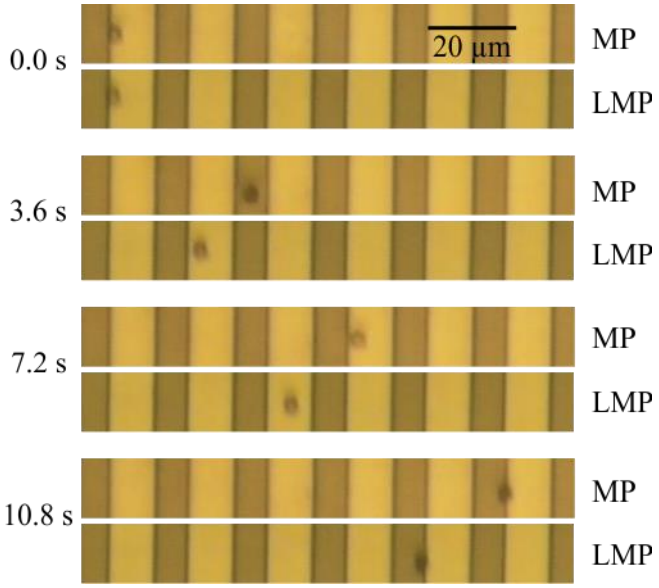

Figure 4.10: Comparison of the bare *micromer®-M-PEG-COOH 3 µm* MP and the LMP with attached 500 nm non-magnetic particles travelling in a G I geometry (c_w = 10 µm, c_s = 8 µm) chip, actuated with a current of I = 50 mA. Actuation times are 2.3 s for the MP and 3 s for the LMP.

5 Conclusions and Outlook

In this thesis a microfluidic biosensing device for detecting a bioanalyte utilizing the motion of magnetic particles (MPs) was presented. The device consists of a microfluidic channel in which MPs are accelerated by a magnetic field gradient generated by current carrying conductors. The detection principle utilizes the effect that MPs with attached analyte (LMPs) have a bigger overall volume while having the same magnetic volume as bare MPs. In consequence LMPs do not reach the same velocity as bare MPs and need more time to travel the same distance while accelerated by the same magnetic field. Calculations were carried out, which provided plausibility for the simulations of magnetic fields generated by straight rectangular conductors, and which showed what amount of velocity decrease can be expected for given MP and analyte diameters.

It was possible to confirm the particle behavior suggested by the calculations and simulations with the experiments that were conducted. Thus the goal of this thesis, to produce a prototype of the described biosensing device and utilize this device to prove the concept of the detection method, was fulfilled.

As already stated in the Introduction, this thesis represents the first part of a three year project. Hence several improvements to the design are possible. The next step is to implement magnetic field microsensors in the device, thus establishing an automated detection of MPs. Different conductor structures may be investigated for the generation of the magnetic field. The contact pads of the conductors could be contacted by wire bonding instead of using copper wire and conductive epoxy, and the chip could be placed in a microchip package.

Appendix

Device masks

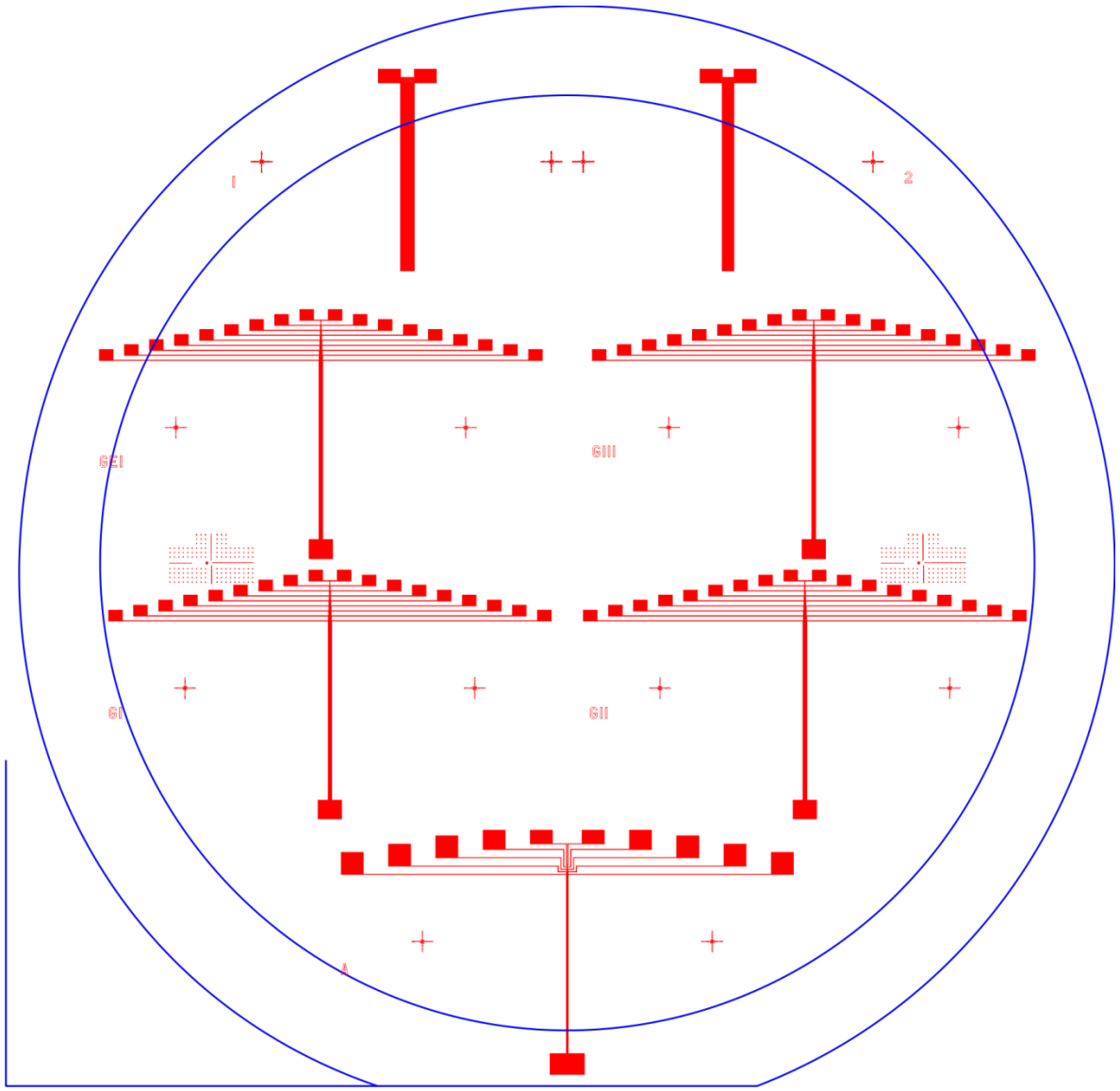

Figure A.1: Full wafer mask for patterning of the conductor microstructures

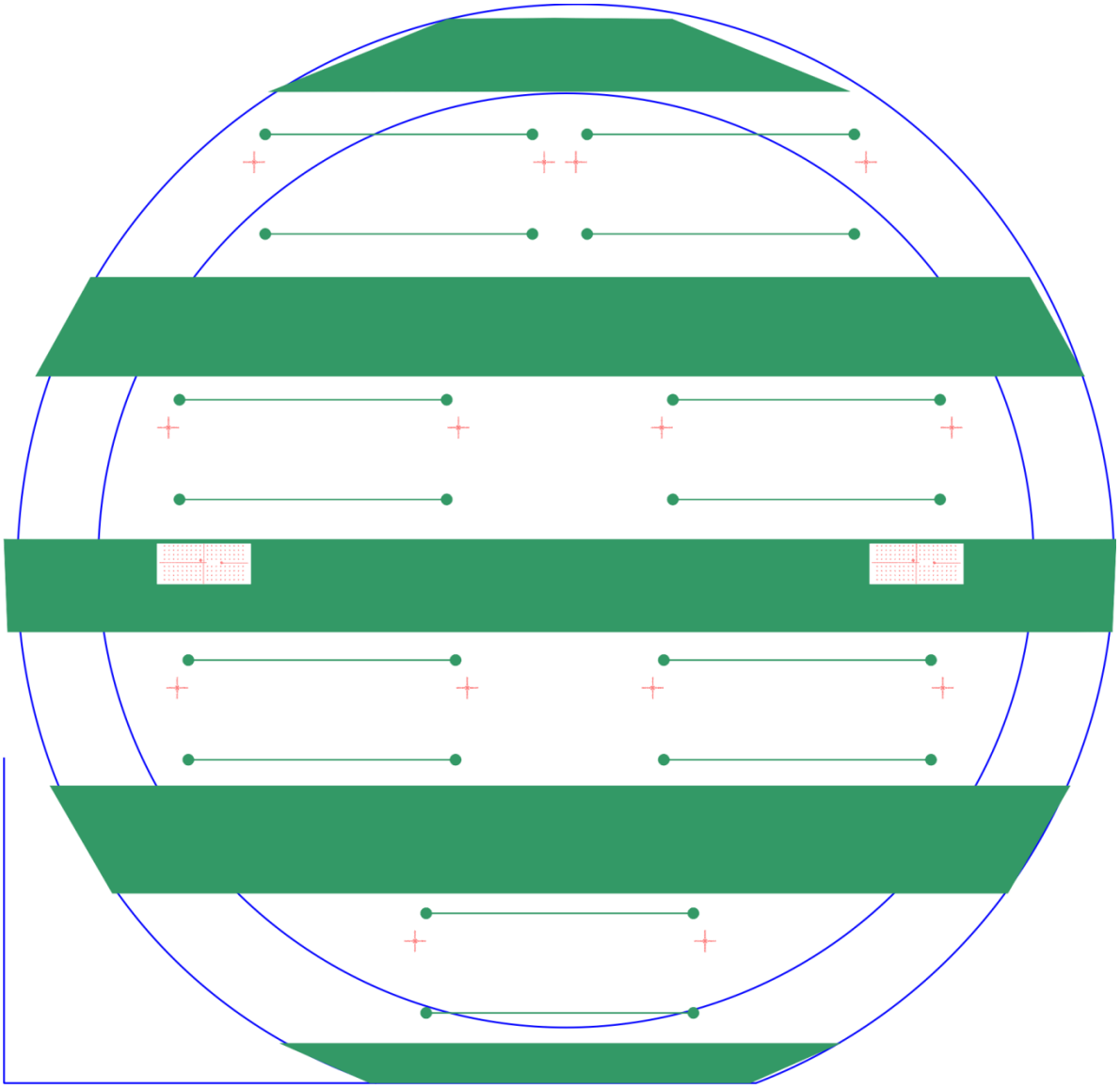

Figure A.2: Full wafer mask for patterning of the microfluidic channels

Conference Papers

In vitro biosensing based on magnetically induced motion of magnetic nanoparticles

A. Dangl, G. Kokkinis, F. Keplinger and I. Giouroudi*

* Institute of Sensor and Actuator Systems, Vienna University of Technology, Gusshausstrasse 27-29/366-ISS, 1040, Vienna Austria, ioanna.giouroudi@tuwien.ac.at

ABSTRACT

This paper presents a method for in-vitro detection of bioanalyte[1] using conductive microstructures to move magnetic nanoparticles (MAPs) in an integrated microfluidic system. The fundamental idea behind the elaboration of such a biosensing system is that the induced velocity of MAPs in suspension, while imposed to a magnetic field gradient, is inversely proportional to their volume [1-2]. Therefore, the volumetric increase of MAPs due to binding of bioanalyte onto their surface, changes consequently the velocity of the MAPs. The resulting compounds, called loaded MAPs (LMAPs), which consist of the MAPs and the attached bioanalyte, need more time to travel the same distance compared to bare MAPs (smaller). Thus, when a liquid sample is analyzed and a change in the velocity of the MAPs occurs the bioanalyte presence in the liquid under examination is demonstrated.

Keywords: biosensors, microfluidics, magnetic particles, velocity change

1 INTRODUCTION

On-chip biosensing and bioanalytical devices based on magnetic methods have attracted significant interest in recent years [3-6]. Specifically, by employing magnetism in biomedical applications automation, fine-tuning and miniaturization are enabled. Moreover, such devices have remarkable advantages over laboratory operated methods such as extraordinary decrease in volumes of sample and reagents that need to be used, minimization of human intervention and low cost fabrication. Finally, in comparison to other on-chip biomedical analysis procedures, magnetic methods do not require additional elaborate equipment, but simply a field gradient generated by a permanent magnet or a specially designed electromagnet.

However, one of the greatest challenges in on-chip biosensing utilizing magnetic methods is to develop micro-sized magnetic field generators. They need to produce magnetic field gradients strong enough to move the MAPs, which can be attached to bioanalyte, towards a sensing area and to be integrated to microfluidic systems.

The presented biosensing system addressed this challenge; the motion was achieved through sequentially actuated, conductive microstructures, controlled by a programmable microprocessor. The advantage of these microstructures over an external permanent magnet was that they ensured a better control of the magnetic field gradient hence allowing uniformity regarding the acceleration of the MAPs. In addition to that, the conductive microstructures were integrated in a complete microsystem. In this paper, magnetic field density calculations and numerical simulations by COMSOL Multiphysics are presented. Additionally, the behavior of MAPs with different diameters under the influence of the applied magnetic field gradient was simulated in order to define the optimum geometry of the conductive microstructures. Finally, preliminary experiments for the proof of sequential acceleration of the MAPs are reported.

2 CALCULATIONS & SIMULATIONS

The magnetic flux density caused by a rectangular conductor with thickness t = 1 μm and width w = 10 μm, running a current of I = 500 mA was calculated in MATLAB. The same scenario was also simulated with COMSOL Multiphysics 4.3. Then the analytical calculated and the simulated values were compared along two different lines (called cut lines in COMSOL) contiguous to the conductor (see Fig. 1):

- along the y-axis at the center (x = 0) of the conductor (see Fig. 2 , red cut line in Fig. 1)
- along the y-axis at the edge (x = 5 μm) of the conductor (see Fig. 3, black cut line in Fig. 1)

It can be seen that the values retrieved from the analytical calculation and the simulation are identical, which indicates that the simulation with COMSOL is plausible.

The principle design of the biosensing system consisted of a microfluidic measurement channel with one inlet and one outlet, a reference channel with one inlet and one outlet and below them the current carrying microstructures to establish the needed magnetic field gradient. These microstructures consisted of parallel straight rectangular conductors, on which current was sequentially applied controlled by a programmable microprocessor.

[1] The word "bioanalyte,, is used throughout this document as a general definition for biomolecules, cells and viruses and is utilized only in order to facilitate the reader.

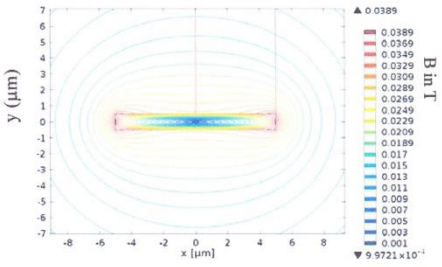

Figure 1: Contour plot of the magnetic flux density caused by a rectangular conductor (1 × 10 µm) running a current of 500 mA, including cut lines (red and black) at which the analytical and simulated values were compared.

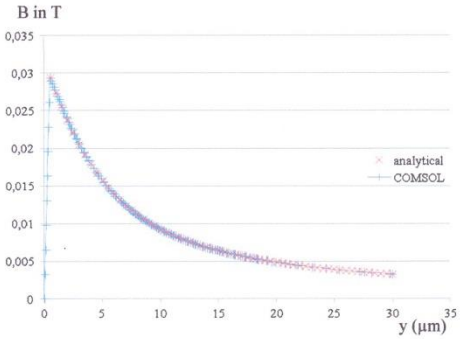

Figure 2: Magnetic flux density calculation (red line) and COMSOL simulation (blue line) along the y-axis at the center of a conductor with dimensions of 1 µm × 10 µm running a current of 500 mA.

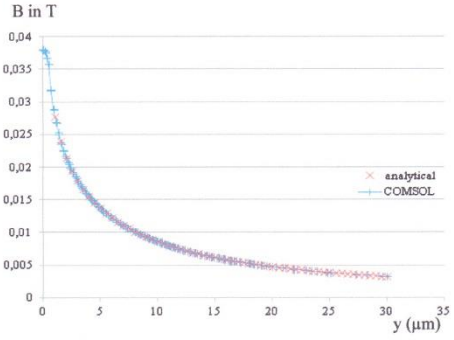

Figure 3: Magnetic flux density calculation (red line) and COMSOL simulation (blue line) along the y-axis at the edge of a conductor with dimensions of 1 µm × 10 µm running a current of 500 mA.

Thus they generated attractive forces on the MAPs and induced their movement along the microfluidic channel from the inlet to the outlet. Several conductor geometries were produced with different conductor widths (c_w) and different distances between the conductors (spacing c_s). Simulations were carried out with COMSOL, to determine which of these geometries is preferable to use. In terms of the current that can be applied to the conductors the joule heating and therefore the current density is the limiting factor. This leaves the conductor thickness (c_{th}) as the last factor that determines the amount of current that can be applied to the different conductor geometries. Two versions were investigated; one with the thickness being 500 nm and the other with the thickness being 1 µm. In a simulation of the joule heating using conductors with a width of 10 µm and a thickness of 1 µm the maximum applicable current was found to be 200 mA, yielding a current density of $J = 2 \cdot 10^{10}$ A/m². Fig. 4 shows the magnetic flux density along the x-axis at a distance of 5 µm from the lower border of a conductor with a width of 10 µm and varying thicknesses (parameter in the plot) and a current density of $J = 2 \cdot 10^{10}$ A/m².

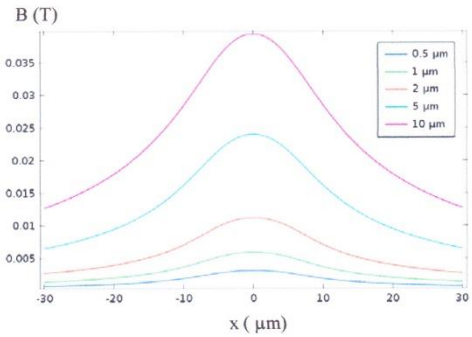

Figure 4: Magnetic flux density along the x-axis at a distance of 5 µm from the lower border of a conductor with a width of 10 µm and varying thicknesses (parameter in the plot) and a current density of $J = 2 \cdot 10^{10}$ A/m².

In practice the maximum achievable conductor thickness is limited by restrictions in the production process; the problem being that the conductors have to be encapsulated in an insulating layer before they can be bonded with the microfluidic channel. Because of the given structure, consisting of parallel conductors separated by predifined distances, the insulating layer does not get an even surface; this effect increases with the conductor thickness. A conductor thickness of 500 nm was found to be the optimum value.

NSTI-Nanotech 2013, www.nsti.org, ISBN 978-1-4822-0586-2 Vol. 3, 2013

3 EXPERIMENTAL

3.1 Working Principle

It has been previously reported that the volumetric increase of MAPs, e.g., due to binding of a bioanalyte onto their surface, changes consequently the velocity of the MAPs caused by a magnetic force [1-2]. The resulting compounds, called loaded MAPs (L MAPs), which consist of the MAPs and the attached bioanalyte, need more time to travel the same distance compared to bare MAPs (smaller). Thus, when a liquid sample is analyzed and a change in the velocity of the MAPs occurs the presence of bioanalyte in the liquid is demonstrated. However, the proof of the novel concept was based on acceleration of the MAPs by a NdFeB permanent magnet of 5 × 5 × 1 mm^3, which was positioned 2 mm outside the microfluidic device. In order to create a compact and portable device a reliable, integrated solution for the motion of the MAPs is required.

3.2 Fabrication Process

First, a photoresist was spin coated, exposed, and developed, for the patterning of the microstructures. Afterwards, 500 nm of silver with a 30 nm adhesion layer of titanium was evaporated on a Si-wafer with a thermally grown oxide. After silver was deposited, the photoresist was stripped using acetone and the remaining debris of the resist was cleaned by oxygen plasma. The silver microstructures consisted of 18 conductors having a 10 μm width and a distance between each of them of 8 μm. An insulating layer of SiO_2 with 1 μm thickness was sputtered on top of the conductors and dry etching was employed to free the bonding pads. The usage of SiO_2 has an additional benefit. According to [7] a layer of SiO_2 produces a negatively charged surface in aqueous buffer, thus producing a repulsive force between negatively charged particles and the solid surface. Thus, particle-solid surface adhesion can be prevented and the MAPs getting stuck at the conductor edges.

Finally, two microfluidic channels were fabricated on top of the conductors; one utilized as a reference channel for the reference sample and the other utilized as the measurement channel. A standard photolithography process and a dry photoresist thin film (Ordyl SY355) of 55 μm thickness (see Fig. 6a,b) was utilized.

3.3 Measurement Set-up

The movement of the MAPs was captured by a Samsung VP-HMX20C camcorder mounted on a Carl Zeiss Microscope and a digital image processing method was utilized in order to estimate the velocity of the MAPs (see Fig. 7).

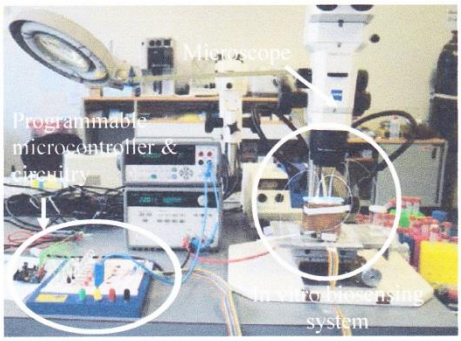

Figure 7: Photograph of the measurement set-up; in vitro biosensing system, programmable microcontroller for the actuation of the conductive microstructures and optical microscope for capturing the movement of the MAPs.

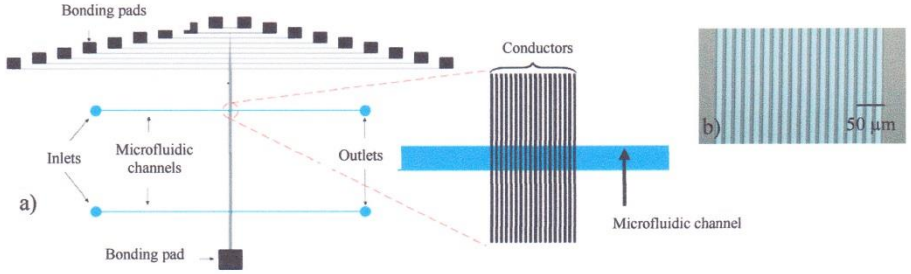

Figure 6: a) Schematic of the in vitro biosensing system consisting of the conductive microstructures and the microfludic channels b) Micrograph of the Ag conductors (10 μm width, 500 nm thickness) fabricated by evaporation on a Si substrate with a top SiO_2 protective layer (200 nm thickness).

3.4 Results and Discussion

2 µl of MAPs (Micromod) coated with carboxylic acid having different diameters (2 µm - 6 µm) with a diluted concentration of 1 mg/ml were injected to the microfluidic measurement channel. A DC current of 50 mA was applied sequentially to each conductor, controlled by the programmable microprocessor. Forces up to 150 pN were obtained at the surface of the conductors. It was proven that by sequentially applying the current to the different conducting elements, the MAPs were moved from the right to the left conductors (see Fig. 8 for MAPs of 6 µm).

The applied magnetic field causes a magnetic moment in the MAPs. The resulting stray magnetic fields can be detected by GMR sensors [8-9]. By integrating one GMR sensor near the inlet of the microfluidic channel a change in the electrical resistance will occur when the MAPs are introduced in the microchannel. Then the MAPs are moved by the applied magnetic field from the silver conductors and as they exit the microchannel another GMR sensor will register a change in its resistance. The time difference between the detection of the resistance change on the first GMR sensor and the detection of the resistance change on the second GMR sensor can be measured. The velocity of the MAPs within the microfluidic channel can then be calculated.

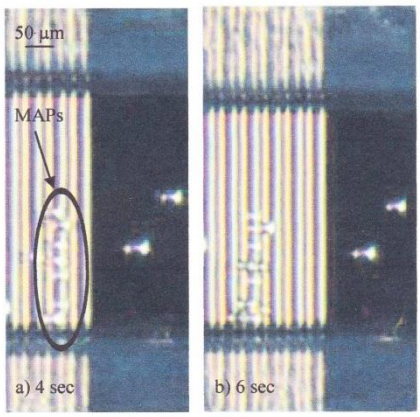

Figure 8: Motion of MAPs with a diameter of 6 µm after sequentially applying current starting from the right conductor towards the left conductors a) 4 seconds and b) 6 seconds.

4 CONCLUSIONS

An integrated solution to continuously move magnetic nanoparticles over a certain distance was obtained by sequentially applying electric current to conductive microstructures arranged in parallel. The presented in vitro biosensing system provides a simple, cost effective and reliable detection method which considerably reduces the measurement complexity. The possibility of using GMR sensors to detect the motion of MAPs is currently being investigated to facilitate an integrated device.

ACKNOWLEDGEMENT

The authors would like to acknowledge the financial support of the Austrian Science Fund (FWF) with Project Nr: P 24372-N19.

REFERENCES

[1] I. Giouroudi, S. Van den Driesche, J. Kosel, Procedia Engineering, 5, 2010.
[2] I. Giouroudi, S. Van den Driesche, J. Kosel, R. Grössinger, M. Vellekoop, J. Appl. Phys. 109, 07B304, 2011.
[3] M. A. M. Gijs, F. Lacharme, and U. Lehmann, Chem. Rev. 110, 1518–1563, 2010.
[4] I. Giouroudi, J. Kosel, Recent Patents on Nanotechnology, 4, 2, 111-118, 2010.
[5] Y.C. Lim, A.Z. Kouzani, and W. Duan, Microsyst Technol, 16, 1995, 2010.
[6] C. Liu, T. Stakenborg, S. Peeters and L. Lagae, J. Appl. Phy, 105, 102014, 2009.
[7] C. Liu, L. Lagae, R. Wirix-Speetjens, G. Borghs, Journal of Applied Physics, 101, 2, 2007.
[8] G.C. P. Gooneratne, Cai Liang, I. Giouroudi, J. Kosel, Journal of Applied Physics, 111, 07B327, 2012.
[9] G. C. P. Gooneratne, I. Giouroudi, J. Kosel, "Microdevice with Half-Ring Shaped GMR Sensors for Magnetic Bead Manipulation and Detection," Lecture Notes in Electrical Engineering: Advancements in Sensing Technology, Edited by S.C. Mukhopadhyay et al., Springer-Verlag, ISBN 978-3-642-32179-5, 2012.

international conference
on materials and applications
for sensors and transducers

http://www.icmast.net

Wednesday, 9 October 2013

Dr Ioanna Giouroudi
Vienna University Of Technology
Institute Of Sensor And Actuator Systems
Gusshausstrasse 27-29/366-ISS
Vienna
1040
Austria
Tel.: +43-1-58801-76691
Fax.: +43-1-58801-36699
Email: ioanna.giouroudi@tuwien.ac.at

Certification of Acceptance

This is to certify that, following a single blinded peer review process, the paper entitled:

Microfluidic biosensing method using the motion of magnetic microparticles
by Mr Georgios Kokkinis, Mr Alexander Dangl, Prof Franz Keplinger and Dr Ioanna Giouroudi

has been accepted for **Oral** presentation at the 3rd International Conference on Materials and Applications for Sensors and Transducers, September 13-17, 2013, Prague, Czech Republic.

This certification is issued to **Mr Georgios Kokkinis, Mr Alexander Dangl, Prof Franz Keplinger and Dr Ioanna Giouroudi** for every legal use.

The Chairmen

Prof Evangelos Hristoforou
National Technical University of Athens

Prof Dimitrios Vlachos
University of Peloponnese

Particle technical data sheets

www.micromod.de Technical Data Sheet Revision Date 24.10.2012 Version 2.2

TECHNICAL DATA SHEET

micromod Partikeltechnologie GmbH

Friedrich-Barnewitz-Str. 4
D-18119 Rostock
Germany

Telephone: + 49 381 / 54 34 56 10
Fax: + 49 381 / 54 34 56 20
E-mail address: info@micromod.de

Product code:	45-00-252
Product name:	Iron oxide particles
Surface:	plain
Size:	250 nm
Solid content:	25 mg/ml
Particle type:	iron oxide particles
Polydispersity index:	< 0.1
Shape:	cluster-typed
Density:	5.35 g/ccm
Magnetization:	46 emu/g iron (H =1000 Oe)
Saturation magnetization:	>71 emu/g iron (H > 10.000 Oe)
Coercive field Hc:	0.481 kA/m
Stable in:	aqueous buffers pH > 4
Not stable in:	organic solvents, acidic solutions pH < 4
Product form:	suspension in water
Particles per ml:	5.7*10E11
Particles per mg:	2.3*10E10
Colour:	dark brown
Additional remarks:	Storage at room temperature.

www.micromod.de Technical Data Sheet Revision Date 24.10.2012 Version 2.2

TECHNICAL DATA SHEET

micromod Partikeltechnologie GmbH

Friedrich-Barnewitz-Str. 4
D-18119 Rostock
Germany

Telephone: + 49 381 / 54 34 56 10
Fax: + 49 381 / 54 34 56 20
E-mail address: info@micromod.de

Product code:	39-00-153
Product name:	sicastar®-M
Surface:	plain
Size:	1,5 µm
Solid content:	50 mg/ml
Particle type:	magnetic silica particles
Shape:	spherical
Density:	2.5 g/ccm
Magnetization:	6.0 emu/g particles (H =1000 Oe)
Saturation magnetization:	> 8.0 emu/g particles (H > 10.000 Oe)
Stable in:	aqueous buffers pH > 3, organic solvents
Not stable in:	hydrofluoric acid, strong basic media, e.g. 6 M NaOH
Product form:	suspension in water
Surface charge density:	5.2 µmol/g
Colour:	dark brown
Additional remarks:	Storage at room temperature.
TECHNOTES:	Isolation of plasmid-DNA: 5-10 µg (from 1-1.5 ml overnight culture), OD (260 nm)/ OD (280 nm) > 1.9.

TECHNICAL DATA SHEET

micromod Partikeltechnologie GmbH

Friedrich-Barnewitz-Str. 4
D-18119 Rostock
Germany

Telephone: + 49 381 / 54 34 56 10
Fax: + 49 381 / 54 34 56 20
E-mail address: info@micromod.de

Product code:	08-01-104
Product name:	micromer®-M
Surface:	NH_2
Size:	10 µm
Solid content:	50 mg/ml
Particle type:	magnetic polystyrene matrix particles
Standard deviation:	< 10 % (C.V.)
Shape:	spherical
Density:	1.1 g/ccm
Magnetization:	1.8 emu/g particles (H =1000 Oe)
Saturation magnetization:	> 2.1 emu/g particles (H > 7.000 Oe)
Stable in:	aqueous buffers, methanol, ethanol, DMSO
Not stable in:	halogenated hydrocarbons, toluene, strong acidic solutions, eg 10% HCl
Product form:	suspension in water
Particles per ml:	8.7*10E7
Particles per mg:	1.7*10E6
Surface charge density:	1 µmol/g
Colour:	dark brown
Additional remarks:	Storage at room temperature.

TECHNICAL DATA SHEET

micromod Partikeltechnologie GmbH

Friedrich-Barnewitz-Str. 4
D-18119 Rostock
Germany

Telephone: + 49 381 / 54 34 56 10
Fax: + 49 381 / 54 34 56 20
E-mail address: info@micromod.de

Product code:	08-56-303
Product name:	micromer®-M
Surface:	PEG-COOH
Size:	3 µm
Solid content:	50 mg/ml
Particle type:	magnetic polystyrene matrix particles
Standard deviation:	< 5 % (C.V.)
Shape:	spherical
Density:	1.1 g/ccm
Magnetization:	5.4 emu/g particles (H =1000 Oe)
Saturation magnetization:	> 6.6 emu/g particles (H > 7.000 Oe)
Stable in:	aqueous buffers, methanol, ethanol, DMSO
Not stable in:	halogenated hydrocarbons, toluene, strong acidic solutions, eg 10% HCl
Product form:	suspension in water
Particles per ml:	3.2*10E9
Particles per mg:	6.4*10E7
Colour:	dark brown
Additional remarks:	Storage at room temperature.

www.micromod.de Technical Data Sheet Revision Date 24.10.2012 Version 2.2

TECHNICAL DATA SHEET

micromod Partikeltechnologie GmbH

Friedrich-Barnewitz-Str. 4
D-18119 Rostock
Germany

Telephone: + 49 381 / 54 34 56 10
Fax: + 49 381 / 54 34 56 20
E-mail address: info@micromod.de

Product code:	01-01-502
Product name:	micromer®
Surface:	NH_2
Size:	500 nm
Solid content:	50 mg/ml
Composition:	polystyrene matrix particles
Polydispersity index:	< 0.2
Shape:	spherical
Density:	1.03 g/ccm
Stable in:	aqueous buffers, methanol, ethanol, DMSO
Not stable in:	halogenated hydrocarbons, toluene, strong acidic solutions, eg 10% HCl
Product form:	suspension in water
Particles per ml:	7.4*10E11
Particles per mg:	1.5*10E10
Surface charge density:	2 µmol/g
Colour:	white
Additional remarks:	Storage at 2 - 8°C.

List of Figures

List of Tables

Literature

[1] I. Giouroudi, S. van den Driesche, J. Kosel, R. Grössinger and M. J. Vellekoop, "On-chip bio-analyte detection utilizing the velocity of magnetic microparticles in a fluid," *Journal of Applied Physics,* vol. 109, no. 7, 2011.

[2] H. Bruus, Theoretical Microfluidics, Oxford University Press, 2008.

[3] M. A. Gijs, F. Lacharme and U. Lehmann, "Microfluidic applications of magnetic particles for biological analysis and catalysis," *Chemical Reviews,* vol. 3, no. 110, pp. 1518-1563, 2010.

[4] N. Pamme, "On-chip bioanalysis with magnetic particles," *Current Opinion in Chemical Biology,* vol. 16, no. 3-4, pp. 436-443, 2012.

[5] A. Weddemann, C. Albon, A. Auge, F. Wittbracht, P. Hedwig, D. Akemeier, K. Rott, D. Meißner, P. Jutzi and A. Hütten, "How to design magneto-based total analysis systems for biomedical applications," *Biosensors and Bioelectronics,* vol. 26, no. 4, pp. 1152-1163, 2010.

[6] "Magnetophoresis," Magnamedics, [Online]. Available: http://www.magnamedics.com/index.php/technology/magnetophoresis. [Accessed February 2013].

[7] N.-T. Nguyen and S. T. Wereley, Fundamentals and Applications of Microfluidics, Artech House, Inc., 2002.

[8] E. Generalic, "Laminar flow. Croatian-English Chemistry Dictionary & Glossary," 24 Jan. 2013. [Online]. Available: http://glossary.periodni.com/glossary.php?en=laminar+flow. [Accessed 20 February 2013].

[9] V. K. Varadan, L. Chen und J. Xie, „Hyteresis loops," in *Nanomedicine; Design and Applications of Magnetic Nanomaterials, Nanosensors and Nanosystems*, John Wiley & Sons, Ltd, 2008, pp. 41-44.

[10] V. K. Varadan, L. Chen and J. Xie, "Single-domain Particles," in *Nanomedicine; Design and Applications of Magnetic Nanomaterials, Nanosensors and Nanosystems*, John Wiley & Sons, Ltd, 2008, pp. 46-47.

[11] B. D. Plouffe, L. H. Lewis and S. K. Murthy, "Computational design optimization for microfluidic magnetophoresis," *Biomicrofluidics,* vol. 5, no. 1, 2011.

[12] C. Liu, L. Lagae, R. Wirix-Speetjens and G. Borghs, "On-chip separation of magnetic particles with different magnetophoretic mobilities," *Journal of Applied Physics,* vol. 101, no. 2, 2007.

[13] "Magnetic Field Gradients," Neuromagnetics Australia Pty Ltd., [Online]. Available: http://www.qmagnets.com/magnetic-field-gradients.php. [Accessed Dezember 2012].

[14] K. Hoshino, Y.-Y. Huang, N. Lane, M. Huebschman, J. W. Uhr, E. P. Frenke and X. Zhan, "Microchip-based immunomagnetic detection of circulating tumor cells," *Lab on a Chip,* vol. 11, no. 20, pp. 3449-3457, 2011.

[15] L. A. Sasso, A. Ündar and J. D. Zahn, "Autonomous magnetically actuated continuous flow microimmunofluorocytometry assay," *Microfluid Nanofluid,* vol. 9, no. 2-3, pp. 253-265, 2010.

[16] W. U. Dittmer, T. H. Evers, W. M. Hardeman, W. Huijnen, R. Kamps, P. de Kievit, J. H. Neijzen, J. H. Nieuwenhuis, M. J. Sijbers, D. W. Dekkers, M. H. Hefti and M. F. Martens, "Rapid, high sensitivity, point-of-care test for cardiac troponin based on optomagnetic biosensor," *Clinica Chimica Acta,* vol. 411, no. 11-12, pp. 868-873, 2010.

[17] H. E. Knoepfel, "Biot-Savart law; Filamentary conductor," in *Magnetic Fields; A Comprehensive Theoretical Treatise for Practical Use*, John Wiley & Sons, 2000, pp. 86-87.

[18] H. E. Knoepfel, "Straight conductors," in *Magnetic Fields; A Comprehensive Theoretical Treatise for Practical Use*, John Wiley & Sons, 2000, pp. 107-110.

[19] "Functionalized micro- and nanoparticles," micromod Partikeltechnologie GmbH, 2012. [Online]. Available: http://www.micromod.de/. [Accessed November 2012].

[20] "About COMSOL Multiphysics," in *COMSOL Multiphysics User's Guide*, 2012, p. 34.

[21] „About Infinite Element Domains and Perfectly Matched Layers," in *COMSOL Multiphysics User's Guide*, 2012, p. 238.

[22] "Rectangle Functions," in *COMSOL Multiphysics User's Guide*, 2012, pp. 189-190.

[23] T. Huesgen, G. Lenk, B. Albrecht, P. Vulto, T. Lemke and P. Woias, "Optimization and characterization of wafer-level adhesive bonding with patterned dry-film photoresist for

3D MEMS integration," *Sensors and Actuators, A: Physical,* vol. 162, no. 1, pp. 137-144, 2010.

[24] P. Vulto, *A Lab-on-a-Chip for automated RNA extraction from bacteria,* Laboratory for Sensors, IMTEK, University of Freiburg, 2008.

[25] "Arduino - ArduinoBoardUno," 2013. [Online]. Available: http://arduino.cc/en/Main/ArduinoBoardUno. [Accessed March 2013].

[26] micromod Partikeltechnologie GmbH, "Technote 200," [Online]. Available: http://www.micromod.de/daten/File/Technotes/Technote_200_1.pdf. [Accessed February 2013].